Multiomics uncovers the epigenomic and transcriptomic response to viral and bacterial stimulation in turbot

Oscar Aramburu [1]*, Belén Gómez-Pardo[1], Paula Rodríguez-Villamayor[1], Andrés Blanco-Hortas[1], Jesús Lamas[1], Pooran Dewari[2], Diego Perojil-Morata[2], Pierre Boudinot[3], Daniel J. Macqueen[2], Carmen Bouza[1], Paulino Martínez[1*]

[1] University of Santiago de Compostela, Spain

[2] The Roslin Institute and Royal (Dick) School of Veterinary Studies, University of Edinburgh, Easter Bush Campus, UK

[3]Université Paris-Saclay, INRAE, UVSQ, VIM, Jouy-en-Josas, 78350, France.

* Corresponding authors

Abstract

Uncovering the epigenomic regulation of immune responses is essential for a comprehensive understanding of host defence mechanisms but remains poorly described in farmed fish. Here, we report the first annotation of the innate immune regulatory response in the genome of turbot (*Scophthalmus maximus*), a farmed flatfish. We integrated RNA-Seq with ATAC-Seq and ChIP-Seq (histone marks H3K4me3, H3K27ac and H3K27me3) using samples from head kidney. Sampling was performed 24 hours post-stimulation with viral (poly I:C) and bacterial (inactivate *Vibrio anguillarum*) mimics *in vivo* and *in vitro* (primary leukocyte cultures). Among the 8,797 differentially expressed genes (DEGs), we observed enrichment of transcriptional activation pathways in response to *Vibrio* and immune response pathways - including interferon stimulated genes - for poly I:C. Meanwhile, metabolic and cell cycle were downregulated by both mimics. We identified notable differences in chromatin accessibility (20,617 *in vitro*, 59,892 *in vivo*) and H3K4me3 bound regions (11,454 *in vitro*, 10,275 *in vivo*) - i.e. marking active promoters - between stimulations and controls. Overlaps of DEGs with promoters showing differential accessibility or histone mark binding revealed a significant coupling of the transcriptome and chromatin state. DEGs with activation marks in their promoters were enriched for similar functions to the global DEG set, but not in all cases, suggesting key regulatory genes were in poised or bivalent states. Active promoters and putative enhancers were differentially enriched in transcription factor binding motifs, many of them common to viral and bacterial responses. Finally, an in-depth analysis of immune response changes in chromatin state surrounding key DEGs encoding transcription factors was performed. This comprehensive multi-omics investigation provides an improved understanding of the epigenomic basis for the turbot immune responses and provides novel functional genomic information that can be leveraged in selective breeding towards enhanced disease resistance.

Keywords: turbot, immune response, epigenomics, chromatin state, transcription factor

INTRODUCTION

The functional annotation of farm animal genomes is important for understanding traits with complex genetic architecture, such as disease resistance, growth, feed efficiency or reproduction (Andersson et al., 2015; Tuggle et al., 2016; Giuffra et al., 2019; Clark et al., 2020). Until recently, functional annotation mainly focused on protein-coding genes using transcriptomics. Transcriptome annotation is now consolidated with robust pipelines (Raghavan et al., 2022) and, throughout the years, transcriptome annotations for human (Frankish et al., 2023), model species (He et al., 2020; Lawson et al., 2020), terrestrial livestock (Summers et al., 2020; Halstead et al., 2021; Overbey et al., 2021) and some aquaculture species (Ramberg et al., 2021; Johnston et al., 2024) have been published.

Non-coding regulatory elements, including promoters, enhancers, silencers and insulators, have been studied in several livestock species but are mostly unexplored in aquaculture species. These elements play essential roles in regulating gene expression and their state can change depending on tissue, cell type, sex, age, and health status (Kellis et al., 2014). Thus, annotation of regulatory elements in different contexts not only aids to address basic questions related to morphology and physiology (Halstead et al., 2020; Pan et al., 2023), but also functional genomic responses to environmental variation (Feinberg, 2007; Ecker et al., 2018; Hu and Barrett, 2017). Genetic variation at non-coding elements also underpins phenotypic variation (Villar et al., 2020; Boltsis et al., 2021), and can thus be leveraged to improve our ability to predict polygenic traits using genomic data (Zhu et al., 2023). In this respect, more than 90% of phenotype-associated single nucleotide polymorphisms (SNPs) identified in human genome-wide association studies (GWAS) are located in non-coding regions (Giral et al., 2018), with similar results reported for livestock (Prowse-Wilkins et al., 2021).

In the past decade, human and livestock functional annotation initiatives have investigated epigenetic mechanisms involved in gene regulation through the study of chromatin state modifications across the genome (Yan et al., 2020a). Chromatin can switch dynamically between active and inactive states in minutes to hours, leaving epigenetic footprints that can be transmitted vertically following DNA replication (Moazed, 2011; Cuvier and Fierz, 2017). Many different sequencing assays have been developed to infer chromatin epigenetic status, including chromatin accessibility (ATAC-Seq; Buenrostro et al., 2015), protein-DNA interactions (ChIP-Seq; Park, 2009) and long-range chromatin interactions (Hi-C; van Berkum et al., 2010). These and other assays are being applied by the FAANG Consortium (Functional Annotation of Animal Genomes; Fang et al., 2019; Foissac et al., 2019; Liu et al., 2020; Clark et al., 2020). Current annotations of chromatin state and regulatory elements remain limited to a few terrestrial farm animal species (Summers et al., 2020, Pan et al., 2021; 2023; Xiang et al., 2021). However, a catalogue of regulatory elements is being generated for several important fish species used in global aquaculture (Johnston et al., 2024), currently the fastest growing animal production sector (Subasinghe et al., 2009; Troell et al., 2023).

Turbot (*Scophthalmus maximus*) is a valuable farmed fish in Europe and Asia (more than 100,000 tons), with the highest production in China (Gao et al., 2023) followed by Spain (APROMAR 2022). Turbot is in its 6th generation of selective breeding and infectious disease outbreaks constitute one of the main challenges this young industry faces (Martínez et al., 2021; Gao et al., 2023). This is a broader trend shared by global aquaculture, where infectious diseases cause losses of totalling more than 5,000 M€ per year (Mishra et al., 2018). Functional annotation of

the turbot transcriptome has been performed against high-quality reference genomes (Figueras et al., 2016; Maroso et al., 2018; Xu et al., 2020; Martinez et al., 2021), including for immune-organs stimulated with viruses (Diaz-Rosales et al., 2012), bacteria (Millán et al., 2011; Libran-Pérez et al., 2022) and parasites (Pardo et al., 2012; Robledo et al., 2014; Ronza et al., 2016; Valle et al., 2020). Candidate genes for disease resistance have been further explored by mapping differentially expressed genes (DEGs) within QTL regions (Martínez, 2016; Saura et al., 2019; Aramburu et al., 2023). However, limited attention has been given to non-coding regulatory elements, beyond a recent analysis of chromatin accessibility focussed on early development (Guerrero-Peña et al., 2023). How chromatin state and non-coding regulatory elements are regulated during immune responses remains undefined in turbot and scarcely explored in other farmed finfish.

The head kidney has been targeted in all previous functional genomics studies in turbot investigating pathogen responses (Millán et al., 2011; Díaz-Rosales et al., 2012; Pardo et al., 2012; Robledo et al., 2014; Ronza et al., 2016; Librán-Pérez et al., 2022; Aramburu et al., 2023), due to its central role in fish immunity (Mokhtar et al., 2023). Head kidney is a key lymphoid organ in most marine fishes and, analogous to the mammalian bone marrow, responsible for the production of high leukocyte diversity, including B-lymphocytes, early-stage T-lymphocytes, as well myeloid cells such as granulocytes and monocytes/macrophages (Klosterhoff et al., 2015; Geven et al., 2017; Chen et al., 2022). Innate immunity provides the first line of defence against pathogens and acts following the binding of pathogen-associated molecular patterns (PAMPs) to germline pattern recognition receptors (PRRs), leading to various effector cellular functions targeting pathogen destruction and clearance.

The aim of this study was to generate the first comprehensive functional annotation of the innate immune response of turbot using a chromosome-level reference genome sequence (Martínez et al., 2021). Live fish and primary immune cell cultures were stimulated using mimics of viral and bacterial infections and compared to controls to capture changes in the transcriptome alongside chromatin accessibility and epigenetic state by integrating RNA-Seq, ATAC-Seq and ChIP-Seq data. Our results provide a deeper understanding of the epigenomic basis for innate immunity in turbot and a novel resource to prioritize genetic variation associated with non-coding elements regulating immune responses.

MATERIALS AND METHODS

Animals

Thirty 8-month-old immature turbot specimens provided by Stolt Sea Farm SA (Ribeira, Spain) were housed in indoor tanks with recirculating seawater at the facilities of the Aquarium of the University of Santiago de Compostela (Spain) for a period of acclimation of 15 d at 16 °C (Supplementary table 1). All fish were fasted for 24 h before stimulations were performed. Eighteen fish were stimulated *in vivo* by intraperitoneal injection, while the other 12 were used for leukocyte isolation for *in vitro* stimulation (see following sections). Fish were anesthetized by bath (MS-222; 100mg/L) and then euthanized by anaesthetic overdose (MS-222; 150 mg/L) before tissue sampling. All animal procedures were approved by the Bioethics Committee of the University of Santiago de Compostela (body authorized according to R.D. 53/2013) and with the authorization of the Xunta de Galicia Regional Government.

Protocols

123 Detailed protocols for the *in vivo* and *in vitro* stimulations, RNA isolation, ATAC-Seq and ChIP-Seq
124 (including library preparation) are available in the FAANG repository (data.faang.org; URLs for
125 protocols in Supplementary tables 1 and 2).

126 ***In vivo* immunostimulation**

127 Six fish were used per experimental condition for the *in vivo* stimulations: i) poly I:C for viral
128 mimic immunostimulation; ii) killed *Vibrio anguillarum* for bacterial immunostimulation; and iii)
129 phosphate buffered saline (PBS) for control. For poly I:C (Sigma P1530), we prepared a working
130 stock at 5 mg/ml in PBS, preheated to 55 °C (15 min) and cooled at room temperature (20 min)
131 before use. Fish were then injected intraperitoneally with 5 µg per g fish weight. For bacterial
132 immunostimulation, an extract of *V. anguillarum* (strain P0382; INRA, France) was used. Bacteria
133 were cultured in a tryptic soy broth medium to an OD600 (optical density at 600 nm) of 1.5. The
134 bacterial pellet (derived from 100 ml of full-grown culture) was washed in an isotonic solution
135 of NaCl (9 g/L) four times and resuspended in 1 ml of the same solution. Bacteria were killed by
136 incubation for 30 sec at 100 °C, allowed to cool at room temperature and stored at -80 °C. The
137 bacteria extract was inoculated in each specimen, diluted in PBS (1:10) for a final volume of 100
138 µl. Control fish were injected with 100 µl of PBS. After 24 h, head kidney samples were extracted,
139 washed with PBS and cut into at least three pieces (> 20 mg each); two were flash frozen on dry
140 ice for ATAC-Seq and ChIP-Seq and the other was immersed in RNAlater (Thermofisher Scientific)
141 for RNA extraction and RNA-Seq. All samples were then stored at -80°C (Figure 1A;
142 Supplementary table 2).

143 ***In vitro* stimulation: leukocyte isolation and culture**

144 Leukocytes were isolated from 12 fish. The entire head kidney was aseptically isolated and placed
145 in a Petri dish with 40 ml of cell isolation media (500 ml of Leibovitz L-15 medium (L-15), 10 ml
146 FBS (2 %), 0.02 % EDTA). Samples were then cut into small pieces and passed through a 100 µm
147 nylon mesh with constant flow of cell isolation media. Leukocytes were separated by
148 centrifugation of 40 ml of the cell suspension gently layered in a 50 ml tube containing 51 %
149 Percoll (400 x g, 30 min, 4 °C, no brakes). The interface layer was collected by centrifugation (400
150 x g, 10 min, 4 °C) and washed three times with L-15 medium containing 0.1 FBS, keeping the
151 pelleted leukocytes (Figure 1B).

152 To ensure enough cells were available, samples were pooled by pairs after cell counting and cell
153 viability was evaluated by the trypan blue exclusion test, totalling 6 pools (each 18 x 10^6 cells;
154 Supplementary table 1). Then, each pool was divided into nine aliquots of 2 x 10^6 cells (in 2 ml)
155 that were dispensed into wells, for a total of 54 wells (6 pools x 9 aliquots): 18 stimulated with
156 20 µl of poly I:C solution; 18 with 20 µl of inactivated *V. anguillarum*; and the remaining 18 wells
157 used as controls (Figure 1B). All leukocyte cultures were incubated for 24 h at 16 °C. Cells were
158 then collected in 2 ml Eppendorf tubes and pelleted at 500 x g for 5 mins at room temperature.
159 Eighteen pellets were resuspended in RNAlater and stored at -80 °C for RNA-Seq, while the other
160 36 were flash frozen in dry ice and stored at -80 °C for ATAC-Seq and µChIPmentation,
161 respectively (Supplementary table 1).
162

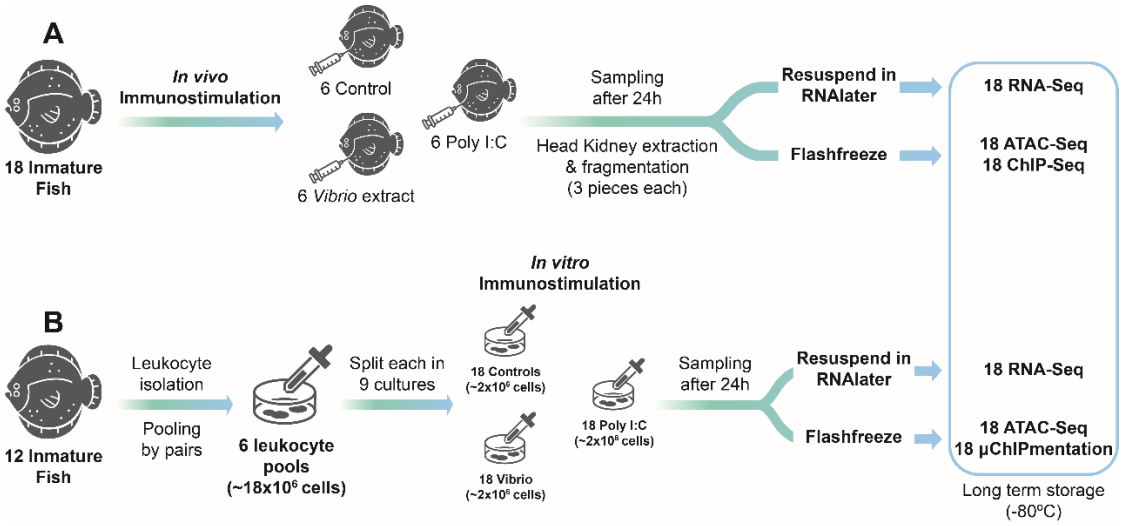

Figure 1. Experimental design followed for turbot immunostimulations: **A)** *in vivo* immunostimulation of immature fish with subsequent sampling of head kidney; **B)** *in vitro* stimulation of head kidney leukocytes of immature fish; 18 samples were used for RNA-Seq, 18 for ATAC-Seq and 18 for ChIP-Seq/µChIPmentation with antibodies to H3K4me3, H3K27ac and H3K27me3 histone marks.

RNA isolation and sequencing

After sample thawing, total RNA was extracted and purified using the miRNeasy Kit (QIAGEN) with specific modifications for: i) frozen head kidney (> 20 mg), following a protocol for "Total RNA extraction for tissues", and ii) frozen leukocytes (2 x 10^6 cells) following a protocol for "Total RNA extraction for frozen cells" (Supplementary table 2). RNA integrity and quantity were evaluated in a Bioanalyzer (Bonsai Technologies, Madrid, Spain) and in a NanoDrop® ND-1000 spectrophotometer (NanoDrop® Technologies Inc., Wilmington, DE, USA). RNA integrity number (RIN) averaged 8.3 across all samples, always above 7.3. RNA samples were delivered to Novogene (UK) for library preparation using NEBNext Ultra Directional RNA Library Prep Kits for Illumina and sequenced using an Illumina NovaSeq S4 platform to generate 150 bp paired end reads.

RNA-Seq data processing

RNA-Seq data was processed using nf-core/rnaseq 3.10.1 (Patel et al., 2023) run with default parameters, using the turbot Ensembl genome ASM1334776v1 (Martínez et al., 2021) as reference. In brief, the pipeline evaluated quality of raw reads using FASTQC (Andrews, 2010) and trimmed adapters and low-quality bases using Trim Galore! (Martin et al., 2011). Reads were then mapped using STAR (Dobin et al., 2013). Normalized transcript read counts were obtained using RSEM (Li and Dewey, 2011). After nf-core processing, the resulting count tables were filtered to remove genes with expression below 5 transcripts per million (TPM < 5) and represented in only one sample across all conditions.

Differential gene expression and gene ontology analysis

Differentially expressed genes (DEGs) between stimulated and control samples were identified using the R/Bioconductor package DESeq2 v1.38.1 (Love et al., 2014). Genes with false discovery rate (FDR) adjusted $p < 0.05$ were considered DEGs. Functional enrichment of the DEG lists was performed using ShinyGO v0.77 (Ge et al., 2020). Gene ontology (GO) terms for Biological

195 Process of each list were ranked by statistical significance (FDR-adjusted $p < 0.05$). All expressed
196 genes across conditions were used as the background for GO analyses.

197 **ATAC-Seq: Library preparation and sequencing**

198 Following a standard protocol for "Nuclei isolation for ATAC-Seq procedures" (Supplementary
199 table 2), the frozen head kidney fragments (> 20 mg; *in vivo* assay) and cell pellets ($2x10^6$ cells;
200 *in vitro* assay) were thawed and resuspended in 1 ml of TST buffer. Each tissue fragment was cut
201 into smaller pieces with a scalpel, mashed with the rubber back of a syringe, and filtered through
202 a 40 µm cell strainer, while cell pellets were resuspended by gentle pipetting. The number and
203 integrity of nuclei was assessed with a haemocytometer (minimum of ~50,000 nuclei in a 16.5
204 µl suspension; ~3,000 nuclei/µl) before carrying out the Tn5 transposase reaction with Illumina
205 Tagment DNA TDE1 enzyme (37°C, 30 min, 1000 RPM, Illumina) following the standard
206 "OmniATAC protocol" (Corces et al., 2017; Supplementary table 2). The resulting DNA was
207 purified with a MinElute PCR purification kit (Qiagen), and DNA concentration assessed with a
208 Qubit using the dsDNA HS kit (ThermoFisher Scientific). Library amplification (10-12 PCR cycles)
209 was carried out using the NEBNext Ultra II DNA Library Prep Kit (New England Biolabs), with IDT
210 for Illumina UD Indexes (96x, Plate A, Set 1, Illumina). Library size selection was performed to
211 remove fragments below 180 bp and above 700 bp using AMPure XP beads (Beckman coulter).
212 Finally, DNA fragment size distribution was assessed with the Bioanalyzer High Sensitivity DNA
213 Assay kit (Agilent Technologies). ATAC-Seq libraries were delivered to Novogene (UK) to be
214 sequenced on an Illumina NovaSeq S4 platform generating 150 bp paired end reads.

215 **ChIP-Seq and µChIPmentation: Library preparation and sequencing**

216 The frozen head kidney fragments (> 20 mg) and leukocyte pellets ($2x10^6$ cells) were thawed on
217 ice. Following a standard "ChIP-seq" protocol (Supplementary table 2), the tissue fragments were
218 transferred into a Douncer homogenizer containing a protease inhibitor cocktail (PIC, Roche, 1
219 tablet in 50 ml of PBS) solution immersed in ice and homogenized using pestles A and B (from
220 less to more plunger adjustment). The leukocyte pellets were resuspended in the PBS and PIC
221 solution. The amount and quality of nuclei was assessed with a haemocytometer and trypan
222 blue staining (> 10 million cells for head kidney; > 100,000 for leukocyte cultures). Due to the
223 low number of nuclei recovered from the leukocyte cultures, a µChIPmentation protocol
224 (Diagenode) was used, following a modified protocol (Supplementary table 2).

225 In both cases, chromatin crosslinking was done using a 1 % formaldehyde solution followed by
226 quenching with glycine (0.125 M). Nuclei were pelleted and resuspended in complete sonication
227 buffer, while leukocyte nuclei were resuspended in Hanks' Balanced Salt Solution (HBSS, Thermo
228 Fisher Scientific) - tL1 buffer (Supplementary table 2). The chromatin was sheared using a Covaris
229 S2 focused ultrasonicator with the following parameters: 2 % duty cycle, intensity 3, with 200
230 cycles per burst, at 4 °C for 8 min and 6 min for head kidney tissue and leukocytes, respectively.

231 The immunoprecipitation was performed using Diagenode antibodies for three marks: H3K4me3
232 (marking active promoter regions; cat. No. C15410003; 1.3 µg/µl), H3K27ac (marking active
233 enhancer and promoter regions; cat. No. C15410196; 2.8 µg/µl) and H3K27me3 (marking
234 Polycomb repressed regions; cat. No. C15410195; 1.1 µg/µl). For head kidney samples,
235 antibodies were coupled with pre-washed protein A and protein G beads, and the tubes left
236 under rotation overnight (~16 h) at 4 °C, following the standard ChIP-Seq protocol. After washing
237 the beads and decrosslinking, the samples were purified using the MinElute PCR purification kit
238 (Qiagen) and later quantified with DNA HS Qubit (ThermoFisher Scientific). Immunoprecipitated
239 chromatin was stored at -20 °C until library preparation, using a Microplex v3 kit (Diagenode).

240 For the leukocyte samples, the µChipmentation kit for histones (Diagenode) was used for
241 chromatin immunoprecipitation and ChIP-Seq library preparation (Supplementary table 2).

242 Before sequencing, the quantity and quality of purified libraries was assessed using the Qubit
243 DNA HS kit (ThermoFisher Scientific) and the High Sensitivity DNA Assay kit (Agilent
244 Technologies), respectively. A minimum of 60 % of the chromatin was required to have a size
245 distribution between 200-700 bp (centered around 350-400 bp). ChIP-Seq libraries were
246 delivered to Novogene (UK) for sequencing on an Illumina NovaSeq S4 platform generating 150
247 bp paired-end reads.

248 **ATAC-Seq and ChIP-Seq data processing**

249 ATAC-Seq and ChIP-Seq data were processed using the nf-core/atacseq v1.2.2. and nf-
250 core/chipseq v1.2.2 pipelines (Ewels et al., 2023), respectively, run with the narrow_peak option
251 for ATAC-Seq and H3K4me3 and H3K27ac ChIP-Seq datasets, and with the broad_peak option for
252 H3K27me3. The other parameters were kept by default. Quality assessment of the reads was
253 carried out with FASTQC (Andrews, 2010), and adapters and low-quality bases trimmed with Trim
254 Galore! (Martin et al., 2011). Reads were mapped to the turbot genome using BWA (Li and
255 Durbin, 2009). Further filtering was done with SAMtools (Danecek et al., 2021), BAMtools
256 (Barnett et al., 2011) and Pysam (Danecek et al., 2021). Genome-wide immunoprecipitation (IP)
257 enrichment relative to controls was done with deepTools (Ramírez et al., 2014) and
258 broad/narrow peaks were called using MACS2 (Zhang et al., 2008). Once nf-core was finished,
259 suboptimal replicates with very low peak numbers were excluded after visualizing their bigwig
260 files on the Integrative Genomics Viewer (IGV; Robinson et al., 2023).

261 **ChIP-Seq and µChIPmentation blacklist**

262 To improve the signal-to-noise ratio of the ChIP-Seq and µChIPmentation data, a blacklist
263 consisting of high signal and low mappability regions was constructed using ChIP-Seq and
264 µChIPmentation inputs, including 21 control ChIPseq turbot samples (ENA accession
265 PRJEB57784). The mappability of the turbot genome for read lengths of 100 bp and 150 bp (k-
266 mers 100 and 150) was quantified using the umap software package (Karimzadeh et al., 2018).
267 The generated mappability files were fed into the ENCODE blacklist software (Amemiya et al.,
268 2019) to generate the blacklist. Alignment and peak files derived from the nf-core pipeline were
269 filtered with BAMtools to remove reads and peaks located in the blacklist regions.

270 **Differential histone modification regions and differentially accessible regions**

271 Differential histone modification regions (DHMRs) and differentially accessible regions (DARs;
272 adjusted $p < 0.05$) between stimulated samples and controls were identified using DiffBind (Stark
273 and Brown, 2011) with default settings.

274 **Integration of ChIP-Seq and ATAC-Seq data with RNA-Seq data**

275 For each condition tested, the promoters of DEGs overlapping with regions tagged as DARs
276 and/or DHMRs were identified. When applicable, a hypergeometric test was performed to check
277 the significance of overlapping between each pair ($p < 0.05$).

278 **Chromatin state inferences**

279 Genome-wide chromatin states for each condition were predicted using ChromHMM (Ernst and
280 Kellis, 2012) integrating the ChIP-Seq data (µChIPmentation for *in vitro* samples) for the three
281 histone marks (H3K4me3, H3K27ac and H3K27me3) and ATAC-Seq data. Chromatin state

prediction was performed by testing ChromHMM models including from 8 to 15 states, keeping the one that returned the most biologically relevant chromatin states, for head kidney and leukocyte data separately (Pan et al., 2021; Baranasic et al., 2022; Vu and Enst, 2022). The genome-wide distribution of resulting chromatin states was visualized on IGV. Regions annotated as enhancer-related states by ChromHMM were retrieved, and each stimulation dataset was compared against its respective control to identify potential enhancer-related regions. Then, each list of regions including potential enhancers annotated as “intergenic” or “intron” were kept as differential enhancer-state regions for further analysis.

Transcription factor motif analysis

Enriched transcription factor (TF) binding motifs (TFBM) included in the HOMER software (Heinz et al., 2010) were identified using the *findMotifsGenome.pl* function (settings: -size given -mask -mset vertebrates) in the different lists of promoter-associated DHMRs/DARs and putative enhancers for each condition. Random genomic regions with GC-content matching each input genomic list were used as the background for automatic motif analysis by HOMER. Only TFBMs with $p < 0.01$ and percentage of target sequences > 5 % were considered enriched.

GO analysis of the TFs predicted to bind enriched TFBMs was performed with Metascape (Zhou et al., 2019) using zebrafish *Danio rerio* as the reference. Finally, a selection of TF genes that were DEGs and contained promoter regions overlapping DARs or DHMRs were explored with IGV (Robinson et al., 2023).

RESULTS

Raw sequencing data and sample metadata

A total of 186 multiomic datasets were produced in this study, including RNA-Seq (36), ATAC-Seq (36) and ChIP-Seq (108; 36 per histone mark, plus 6 ChIP-Seq input controls). Full information on samples and metadata is shared in Supplementary tables 1 and 2.

RNA-Seq

On average, 69,580,246 raw reads per library were produced across the 36 RNA-Seq samples, with 97.2 % mapping to the turbot genome (Supplementary table 3A). Principal Component Analysis (PCA) showed that 77 % of the transcriptome variance was explained by PC1, separating the *in vivo* and *in vitro* stimulations (Figure 2A). Despite all three *in vivo* conditions grouping together, a suggestive spatial segregation was observed mainly across PC1, with the control at one end and the *Vibrio* stimulation at the other. For the *in vitro* stimulations, PC2 clearly separated the *Vibrio* stimulation from poly I:C and control samples, the last two showing some overlap (Figure 2B).

Table 1. Number of differentially expressed genes (DEGs) for the *in vitro* and *in vivo* stimulations with *Vibrio* and poly I:C

Stimulant	Stimulation	Upregulated DEGs	Downregulated DEGs	Total DEGs
Vibrio	*in vitro*	3,321	3,217	6,538
	in vivo	910	929	1,839
poly I:C	*in vitro*	858	544	1,402
	in vivo	2,001	1,918	3,919

Differential expression analysis was performed by comparing each stimulated condition to the respective controls, both for the *in vitro* and *in vivo* stimulations. In total, 8,797 DEGs were identified across all comparisons (Table 1, Supplementary table 4). For the *in vitro* stimulations, a stronger response was observed for *Vibrio* than poly I:C stimulation, both for up and downregulated genes. Meanwhile, poly I:C showed a higher number of DEGs than *Vibrio* for the *in vivo* stimulations both for up and downregulated genes (Table 1, Supplementary table 4). Overall, more DEGs were detected in the *in vitro* than in the *in vivo* stimulations (7,940 vs 5,758, respectively).

Functional enrichment among DEGs

Gene Ontology (GO) analysis identified enriched biological processes for up and downregulated DEGs in all conditions (Supplementary table 5). Among the downregulated DEGs, metabolism, cell cycle and cytoskeleton organization terms were enriched for the *in vitro* stimulations, while a limited number of terms were detected for *in vivo* stimulations (Supplementary table 5).

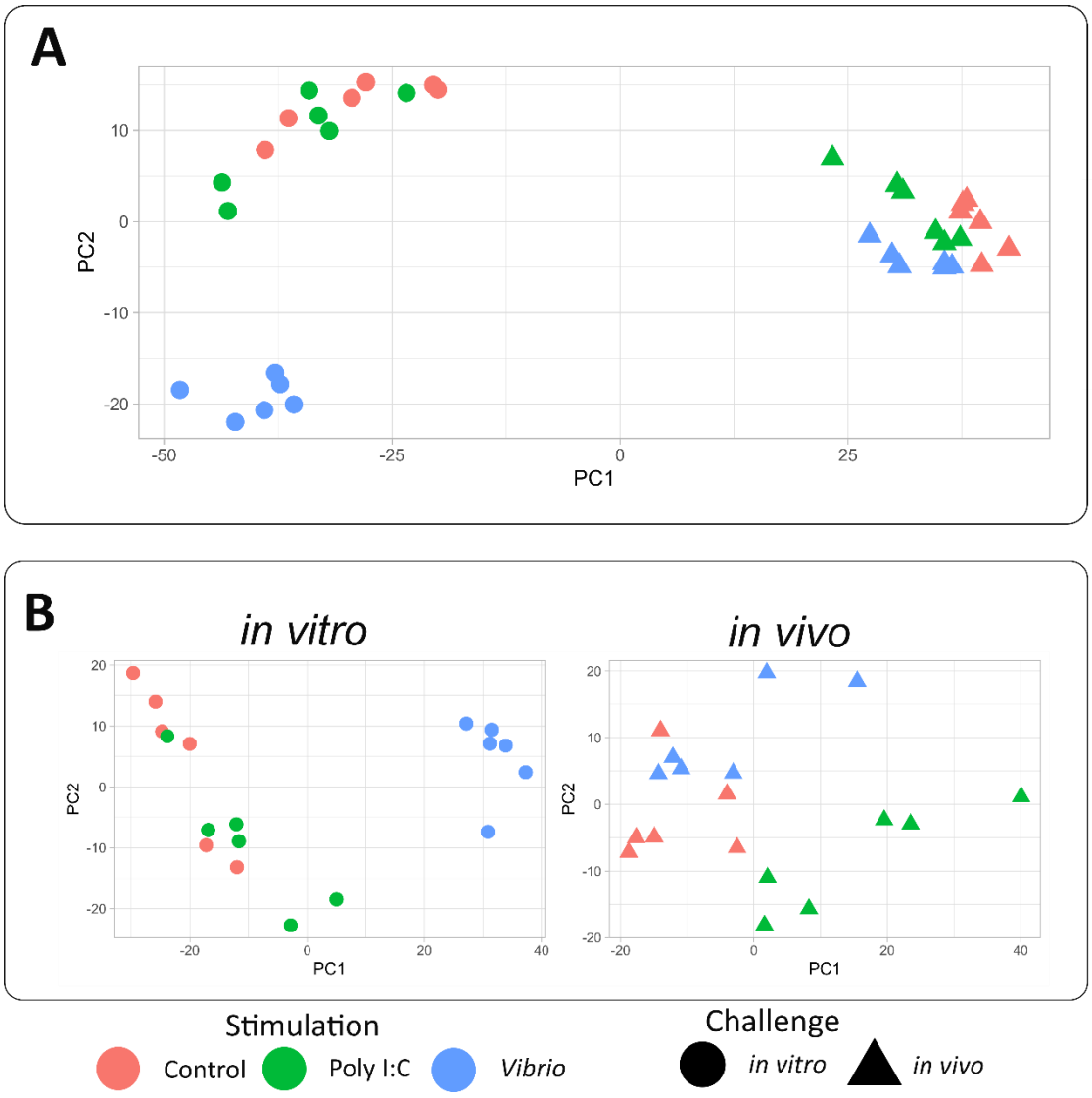

Figure 2. PCA of the *in vivo* and *in vitro* transcriptomic response to stimulation with poly I:C and *Vibrio*. **A)** PCA of the whole transcriptomic dataset; **B)** Independent PCAs for the *in vitro* and *in vivo* transcriptomic assays.

More abundant and specific enriched GO terms were detected among the upregulated DEGs. Although RNA metabolism was enriched for most stimulations, poly I:C stimulation was linked to a more specific activation of key immune functions (particularly *in vitro*) such as interferon-stimulated genes and cytokine pathways, and regulation of toll-like receptors, besides more general immune terms. DEGs for the *in vitro Vibrio* stimulation were enriched for immune-related terms associated with cytokine and several transport pathways, whereas *in vivo* upregulated genes displayed strong enrichment of terms related to cytoskeleton organization, tissue development and syncytium formation (Supplementary table 5).

Comparing DEGs between conditions, important immune-related GO terms were commonly enriched between the *in vitro* poly I:C and *Vibrio* stimulations (Figure 3; Supplementary table 6), including interferon type I stimulated genes (*socs1a, socs1b, nod2, nmi*), cytokine signalling (the same genes plus *traf2*, *stat4* and *il15ra*) and major histocompatibility complex type I (MHC-I) pathways (*erap1b*, *tapbpl*, *tapbp*.2). Activation of transcription, protein localization, and a small number of terms associated with the immune-related "peptidyl-arginine modification" (*prmt1, prmt3, prmt5, prmt7*) were overrepresented *in vivo*.

We detected several DEGs regulated in opposite directions for poly I:C and Vibrio stimulations (Table 2; Figure 3; Supplementary table 6), suggestive of divergent immune responses for bacteria and virus. Among the *in vivo* upregulated DEGs for *Vibrio* and downregulated for poly I:C, we observed enrichment of general immune functions, including genes such as *il-1b*, *traf4a* and *f2r*. Conversely, immune-related genes including *nod2*, *sting1*, *irf1b* and *apaf1*, were downregulated for *Vibrio* and upregulated for poly I:C *in vivo*. Interestingly, most genes involved in the type-I IFN response orthologs of human and mouse (interferome database; Rusinova et al., 2023; Clark et al., 2023) were upregulated in the poly I:C stimulations, while downregulated with *Vibrio* extracts, especially in the *in vivo* stimulation (Table 2).

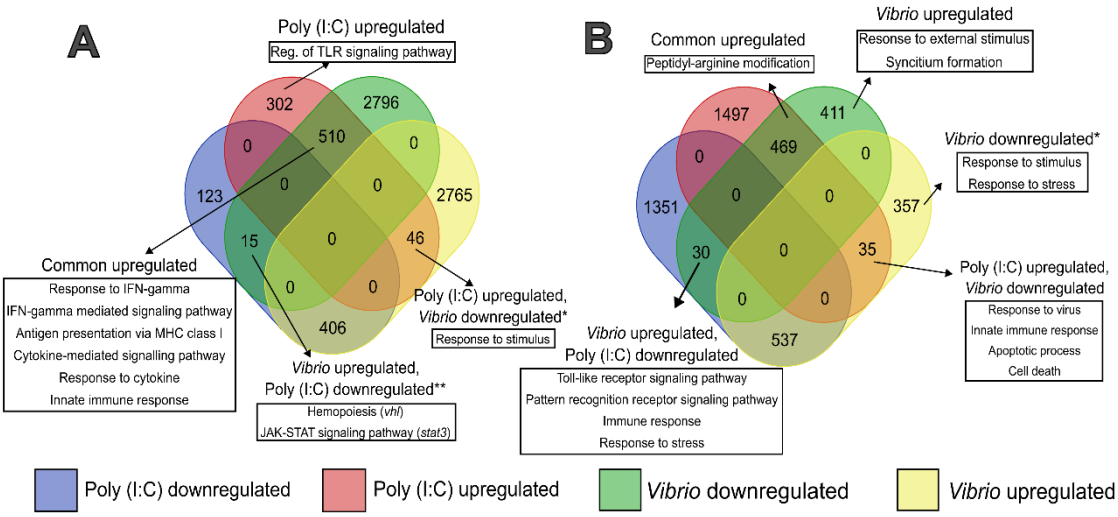

Figure 3. Venn diagrams illustrating overlap of DEGs for: **A)** *in vitro* poly I:C vs *Vibrio*, and **B)** *in vivo* poly I:C vs *Vibrio*. The white boxes show enriched GO terms related to the immune system found in specific subsets. Asterisks (*) highlight cases where suggestive immune-related GO terms were identified, despite not being significantly enriched. Double asterisks (**) highlight specific genes (in parentheses) associated with relevant immune functions. GO terms for the genes in the list were extracted from Ensembl-BioMart.

Table 2. Immune-related DEGs showing opposite responses following *Vibrio* and poly I:C stimulations.

Comparison	Differentially expressed genes (DEGs)
In vitro - upregulated by poly I:C, downregulated by *Vibrio*	***aldh2-like***, ***arhgap22***, *arrdc2*, *asb9-like* ***ascc3***, ***atxn7l1***, *bpifcl*, *c1qa*, ***cep170b***, *chaf1b*, *cnnm4b*, ***dync1h1***, ***ece2b***, ***ermp1-like***, ***gna14***, ***gpr155a***, ***has1***, ***ip6k2-like***, ***mapk8a***, ***mycbp2***, *nfkb1*, ***notch2***, *pld4-like*, *psda*, *rilp*, *serinc1-like*, *sgk2b*, *sp100.1*, ***spsb4a***, ***sptbn1***, *stim2b*, *synpr*, ***tank***, *tent4b*, ***tlr8***, *tmem269-like*, *tnk2b*, *tpm4b*, ***trim25-like***, ***trim35-14***, ***usp1***, *vcanb*
In vitro - upregulated by *Vibrio*, downregulated by poly I:C	*bcat-like*, *ctns*, *gid8b-like*, *pcxb*, ***psat1***, *rab11b-like*, *rtf2*, *sfxn2*, ***slc25a43***, ***stat3***, *thoc7*, *tollip*, *vhl*, *vps26c*, *vps41*
In vivo - upregulated by poly I:C, downregulated by *Vibrio*	*adora4a*, ***ankrd10b***, ***apaf1***, *arhgap12b*, *atg9a*, ***atxn7l1***, *bpifcl*, *camkk1b*, ***casp1a-like***, *cylda*, *emilin1*, ***fem1c***, *gfral*, ***gna14***, *gnptab*, *il22ra2*, ***irf1b***, *nlrc3-like*, ***nod2***, *nsmce4a*, *otulina*, ***parp15-like***, ***pstpip1b***, ***pstpip2***, ***rasgef1b***, *rnf146*, ***rnf170***, ***sting1***, ***themis2***, ***txk***, *ubp15*, *ucp2-like*, ***xcr1-like***, ***xkr8-like***
In vivo - upregulated by *Vibrio*, downregulated by poly I:C	*aebp1*, *alpl*, *anxa13l*, *anxa1a*, *cald1a*, *capn2b*, *chchd6a*, *col17a1-like*, *f2r*, *ggh-like*, *icn-like*, *il-1b*, *il8-like*, *il11-like*, *kdm2aa*, *lims2*, *map1lc3b*, *mfsd10*, *msto1*, *olfm5-like*, *osbpl10*, *plpp1like*, *plxnb2b*, *slc4a4-like*, *tlr13-like*, *traf4a*, *vat1*, *zan-like*

Turbot orthologs of human/mouse type I IFN stimulated genes (ISG) are highlighted (in bold upregulated and underlined downregulated), based on the database Interferome (Rusinova et al., 2013) and Clark et al. (2023). Note that most of these genes are downregulated in response to Vibrio anguillarum.

Considering condition-specific DEGs (Figure 3; Supplementary table 6), upregulated by poly I:C *in vitro* DEGs were enriched for terms associated with toll-like receptor signalling pathway (*usp4, tasl, irak3*), while transcriptional activation terms were found among DEGs in *Vibrio in vitro.* For the *in vivo* stimulations, transcriptional activation GO terms were enriched for upregulated DEGs after poly I:C stimulation, whereas response to stimulus (explained by *tlr3, hamp, tnip1, fxc1a* and *ccr12a*, among other genes) and syncytium formation (explained by *kirrel3l*, *jam2a*, *plekho1b*) were enriched for *Vibrio*.

ATAC-Seq and ChIP-Seq

Excluding some ATAC-Seq *in vitro* libraries not associated with the stimulant, most libraries showed > 95% read mapping to the turbot genome (Supplementary table 3B). On average, we identified 24,251 (*in vitro*) and 62,013 (*in vivo*) peaks per sample for ATAC-Seq; 26,199 (H3K4me3), 13,461 (H3K27ac) and 27,765 (H3K27me3) peaks for the *in vivo* ChIP-Seq data; and 15,870 (H3K4me3), 5,363 (H3K27ac) and 38,784 (H3K27me3) peaks for the *in vitro* ChIP-Seq data. Samples in the PCA plot were mostly segregated across PC1, although PC2 explained most of the variance between histone marks, particularly differentiating repressive (H3K27me3) from active (H3K4me3 and H3K27ac) marks (Figure 4). *Vibrio* showed the greatest differentiation

among the stimulations, while poly I:C and controls were mostly intermingled, particularly for ATAC-Seq (*in vitro* and *in vivo*) and H3K4me3-ChIP-Seq (*in vitro*).

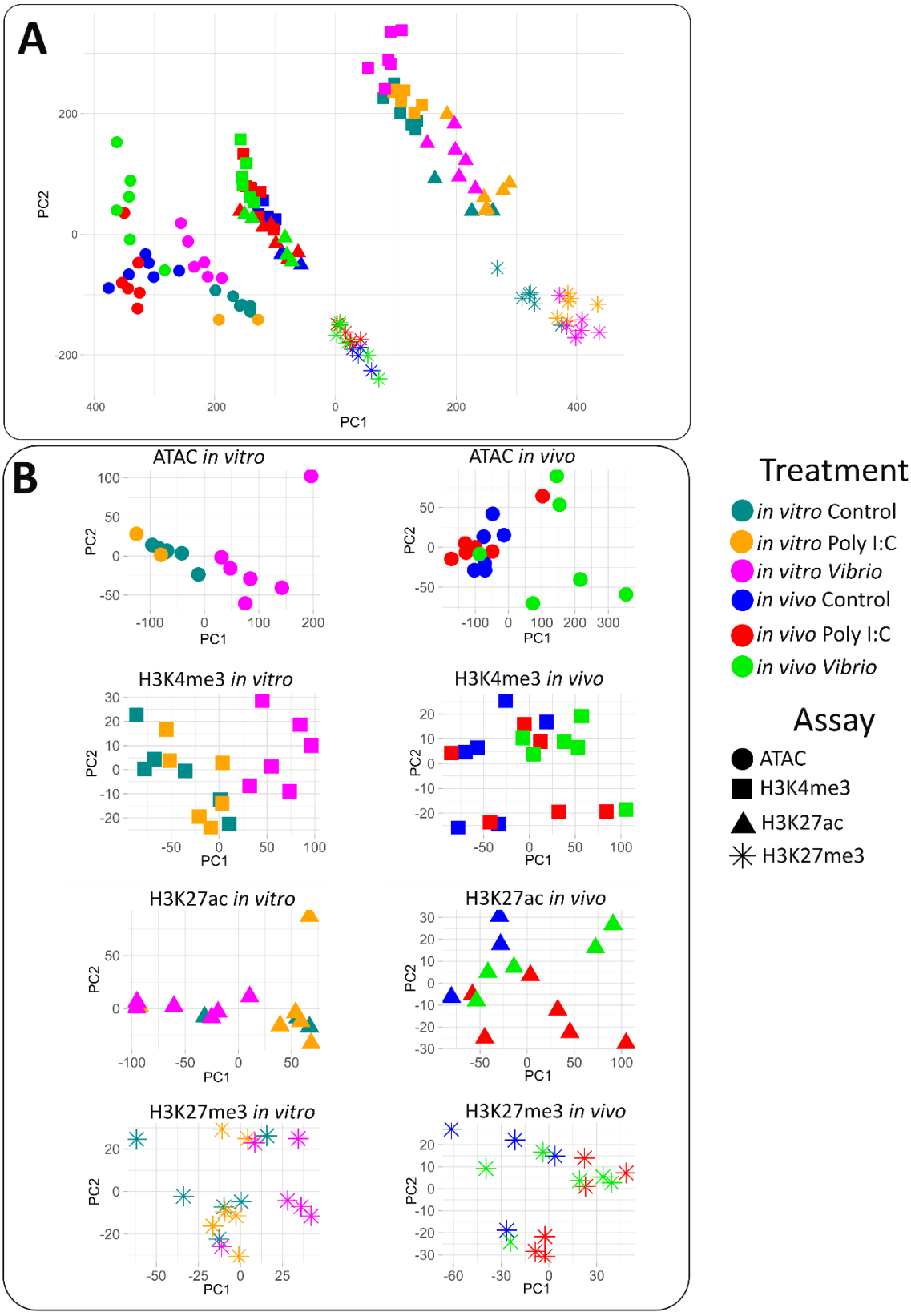

Figure 4. PCA of the *in vivo and in vitro* epigenomic response to stimulation with poly I:C and *Vibrio*. **A)** PCA of the whole dataset; **B)** Separated PCAs for each assay and condition.

ChIP-Seq blacklist

Certain genomic regions obscure epigenetic analyses because of anomalous, unstructured, or high signal due to particular genomic features (Amemiya et al., 2019). Using the 21 ChIP-Seq and µChIPmentation input controls (ENA project PRJEB57784) we constructed a blacklist of low confident genomic regions for turbot ChIP assays (Supplementary table 7). On average, 6.98 % (~39Mb) of the turbot genome was included in the blacklist, consisted of high input signal (5.58 %) and low mappability (1.40 %) regions (Supplementary figure 1).

Chromatin state annotation

Genome-wide chromatin state predictions were produced using ChromHMM employing the ChIP-Seq and ATAC-Seq data from stimulated and control samples from head kidney and leukocytes (Figure 5, Supplementary table 8). For the *in vivo* head kidney samples (Figure 5A), a 10-state model was chosen including promoters/transcription start sites (TSS; States 1, 2, 3 and 4), potential enhancer regions (States 5 and 6), ATAC islands (State 7, i.e. ATAC-peaks lacking histone marks), repressed regions (States 8 and 9) and low signal regions (State 10). For the *in vivo* leukocytes (Figure 5B), an 8-state chromatin model was chosen including promoters/TSS (States 1, 2 and 3), potential enhancer regions (States 4 and 5), ATAC islands (State 6), repressed regions (State 7) and low signal regions (State 8). For each chromatin state map, ±2kb regions around the TSS showed signal specifically for chromatin states 1, 2, 3 and 4 for head kidney (*in vivo*) and states 1, 2 and 3 for leukocytes (*in vitro*), mostly corresponding to promoter regions and/or transcriptionally active regions.

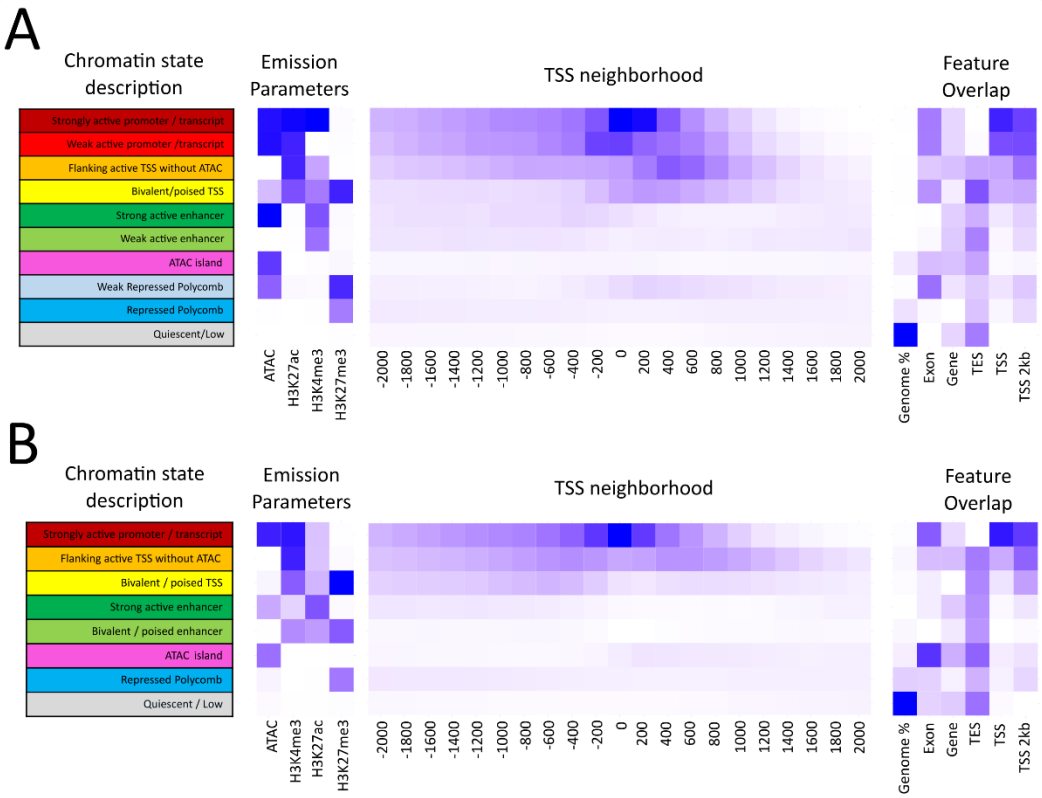

Figure 5. Chromatin state models of the turbot genome: **A)** 10-state model based on *in vivo* samples; **B)** 8-state model based on *in vitro* samples. Heatmaps of the emission parameters for each chromatin state are shown for ChIP-Seq data with three histone marks and ATAC-Seq (left), the neighbourhood around the TSS (middle) and the emission parameters of each chromatin state considered alongside features within the turbot genome (right). TSS: Transcription start site; TES: Transcription end site.

415 **Differential chromatin accessibility regions (DAR) and differential histone modification regions**
416 **(DHMR) following stimulation**

417 We next aimed to identify regulatory regions in the turbot genome affected by the immune
418 stimulation. Significant DARs and DHMRs (FDR-adjusted $p < 0.05$) contrasting *Vibrio* and poly I:C
419 stimulations to control samples were identified (Table 3, Supplementary table 9). Globally, a
420 higher number of DARs or DHMRs were detected for up- than for down-regulated regions, more
421 *in vivo* than *in vitro*, and more for *Vibrio* than poly I:C comparisons. Additionally, histone marks
422 H3K27ac and H3K27me3 showed much lower DHMRs than H3K3me3 or ATAC-Seq DARs.

423 **Table 3.** Differential Accessibility Regions (DARs) and Differential Histone Modification Regions (DHMRs)
424 for the *in vitro* and *in vivo* immune stimulations with viral and bacterial PAMPs

PAMP	Stimulation	Assay	Upregulated DAR/DHMR	Downregulated DAR/DHMR	All DAR/DHMR
Vibrio	*in vitro*	ATAC	17,878	2,739	20,617
		H3K4me3	10,755	699	11,454
		H3K27ac	623	2	625
		H3K27me3	1,211	6	1,217
	in vivo	ATAC	16,733	43,159	59,892
		H3K4me3	9,988	287	10,275
		H3K27ac	3	0	3
		H3K27me3	0	4	4
poly I:C	*in vitro*	ATAC	0	0	0
		H3K4me3	0	0	0
		H3K27ac	20	0	20
		H3K27me3	0	0	0
	in vivo	ATAC	15	25	40
		H3K4me3	1,036	0	1,036
		H3K27ac	38	0	38
		H3K27me3	0	126	126

425

426 **Association of ATAC-Seq and ChIP-Seq data with RNA-Seq data**

427 We tested if DARs and DHMRs for H3K4me3 and H3K27ac marks annotated as promoter/TSS
428 regions (up to -1kb upstream of TSSs) corresponded to DEGs under the same experimental
429 conditions (Hypergeometric distribution test, $p < 0.05$). DARs and DHMRs were much more
430 overrepresented at the promoter regions of up- rather than down-regulated DEGs (Table 4,
431 Supplementary table 10), suggesting changes in chromatin state associated with activation of
432 genes. We performed GO enrichment analyses of DEGs overlapping with DARs and DHMRs for
433 activation marks (H3K4me3 and H3K27ac) at promoter regions within each experimental
434 condition through Hypergeometric distribution tests ($P < 0.05$, Table 4). Significant enrichment
435 was detected for upregulated genes ($p < 0.05$), including several metabolic activities and
436 particular immune functions, including antigen processing/presentation and apoptotic/cell
437 death pathways (Supplementary table 11). Specifically, enriched terms were mostly associated
438 with RNA processing (in particular tRNA, rRNA, ncRNA), ribosome biogenesis, and translation for
439 the *Vibrio in vitro* stimulation, whereas for protein localization to nucleus and organelle, DNA
440 replication and carbohydrate metabolism for the *Vibrio in vivo* stimulation. The term 'peptidyl-
441 arginine modification' was enriched for the intersection of DAR/DHMRs and DEGs (*prmt1, 3, 5*

442 and *7*), as outlined before for the whole DEG analysis (RNA-Seq). The poly I:C *in vivo* stimulation
443 showed enrichment in immune-related processes, including 'antigen processing and
444 presentation via MHC-I' (explained by *erap1b, tapbpl*) and 'regulation of programmed cell death'
445 (explained by *apaf1, bida, casp8 and 10, socs3a, grinab, bcl2l10*; Supplementary table 11).
446

447 **Table 4.** Overlap of promoter DARs and DHMRs with DEG promoters (Hypergeometric test, $p < 0.05$).
448 Significant results are underlined. Refer to Supplementary table 10 for further details.

Experimental condition	DARs/DHMRs at promoter regions		Integration of DARs/DHMRs at promoter regions of DEGs			
			Down		Up	
	Down	Up	DEG	DAR/DHMR + DEG	DEG	DAR/DHMR + DEG
ATAC poly I:C *in vitro*	-	-	544	-	858	-
ATAC *Vibrio in vitro*	55	4922	3217	1	3321	1259
ATAC poly I:C *in vivo*	4	1	1918	0	2001	0
ATAC *Vibrio in vivo*	1350	6115	929	34	910	395
H3K4me3 poly I:C *in vitro*	-	-	544	0	858	0
H3K4me3 *Vibrio in vitro*	53	4289	3217	14	3321	1164
H3K4me3 poly I:C *in vivo*	-	368	1918	-	2001	151
H3K4me3 *Vibrio in vivo*	22	4024	929	3	910	242
H3K27ac poly I:C *in vitro*	-	0	544	-	858	0
H3K27ac *Vibrio in vitro*	0	72	3217	0	3321	49
H3K27ac poly I:C *in vivo*	-	4	1918	-	2001	3
H3K27ac *Vibrio in vivo*	-	1	929	-	910	1
Active prom poly I:C *in vitro*	-	-	544	-	858	-
Active prom *Vibrio in vitro*	106	6744	3217	15	3321	1782
Active prom poly I:C *in vivo*	4	370	1918	0	2001	151
Active prom *Vibrio in vivo*	1263	7082	929	37	910	463

449 *prom: promoter; DAR: differential accessibility regions; DHMR: differential histone modification regions*

450 **Transcription factor binding motif (TFBM) analysis**

451 To establish TFs potentially associated with chromatin state regulation following immune
452 stimulation, the enrichment of TFBMs within DAR/DHMRs annotated as promoter or enhancer
453 regions were examined. Significant enrichment was detected for poly I:C *in vivo* and the *Vibrio*
454 *in vitro* and *in* vivo stimulations. On average across simulations, 4 (range: 0-11) and 71 (range: 0-
455 132) enriched TFBMs were detected for down- and upregulated promoters, respectively, while
456 14 (range: 6-27) and 49 (range: 1-80) respective TFBMs were enriched for downregulated and
457 upregulated enhancers (Supplementary table 12).

458 Most TFBMs and associated TFs predicted for active promoters and enhancers were enriched for
459 several stimulations (Figure 6; Supplementary table 12): 68 TFs for both *Vibrio* stimulations and
460 *in vivo* poly I:C; 59 TFs for both *Vibrio* stimulations; and 20 TF for both *in vivo* stimulations.

461 To further investigate the functions of TFs with enriched motifs, we used the Molecular Complex
462 Detection algorithm (MCODE) and protein-protein interaction data (PPI) to identify connected
463 functions among differentially expressed TFs and among TFs with DARs or DHMRs on their
464 promoters (Table 5, Figure 7, Supplementary Figure 2).

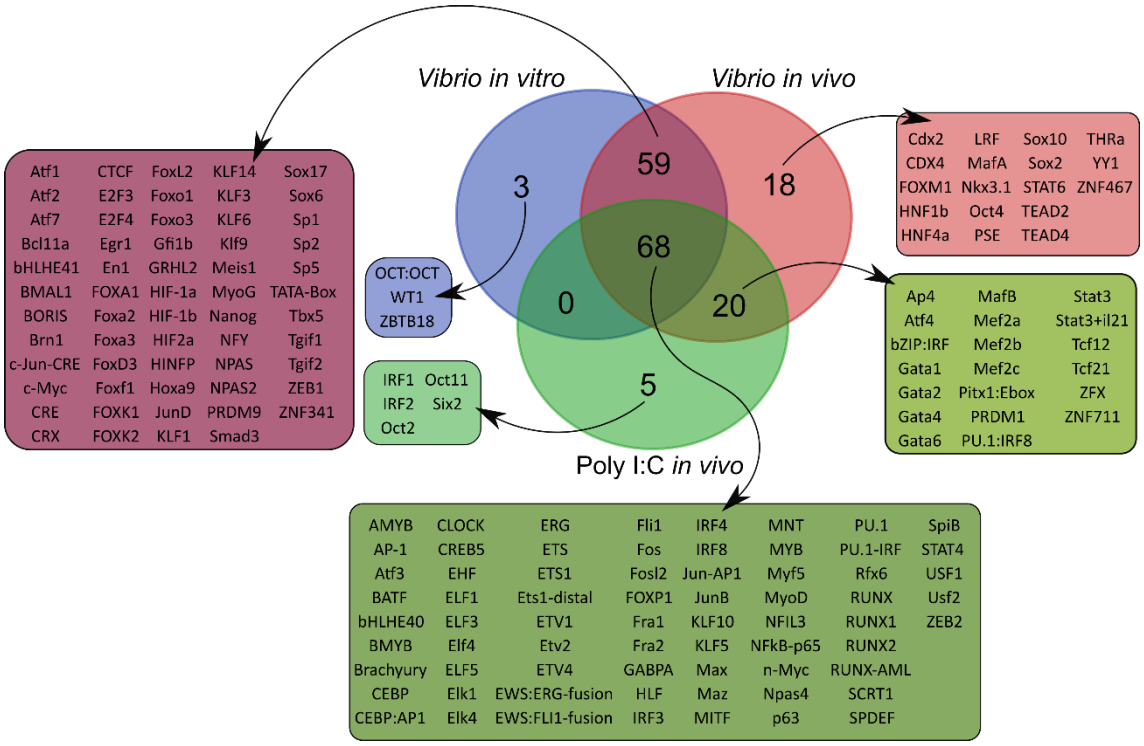

Figure 6. Venn diagram illustrating overlap of enriched transcription factor binding motifs (TFBMs) in upregulated promoter and enhancer regions in response to the different stimulants. Each coloured box shows the TFBM found.

Table 5. Upregulated TFs with binding motif enrichment predicted on DARs and DHMRs (H3K4me3 and H3K27ac) of active promoters and enhancer regions. The second column shows TF with promoters overlapping with DAR/DHMR, while the third column shows TF that are differentially expressed genes (DEGs). TF that are in both columns are underlined.

Stimulation		Transcription factor DAR/DHMR	Transcription factor DEG
poly I:C	*in vitro*	-	-
	in vivo	BATF, BHLHE40, PU.1, RUNX1, ZEB2	ELK4, ETV4, FRA1, IRF1, IRF8, MEF2C, PU.1, STAT3
Vibrio	*in vitro*	AP1, ATF1, BATF, BCL11A, BHLHE40, BHLHE41, BMYB, JUN, MYCA, EGR1, ELK1, EN1, FOS, FOSL2, FOXK1, FOXK2, FOXO1, FOXO3, FRA2, HIF1A, HIF1B, HINFP, IRF3, IRF4, IRF8, JUNB, JUND, KLF6, KLF9, MEIS1, MITF, MNT, MYB, NFkB-p65, PU.1 RUNX1, SMAD3, SP1, SP2, STAT4, USF1, USF2, ZEB2, ZNF341	ATF3, BHLHE40, BMYB, MYCA, ELF3, FOXO1, FOSL1A, FRA1, HIF1B, IRF3, IRF8, MITF, p63, STAT4
	in vivo	AP1, ATF1, ATF2, ATF4, ATF7, BATF, BCL11A, BHLHE49, BMYB, JUN, MYCA, CRE, EGR1, ELK1, EN1, ETV4, FOS, FOSL2, FOXK2, FOXO1, FOXO3, FRA2, HIF1B, HINFP, IRF3, IRF4, IRF8, JUNB, JUND, KLF6, KLF9, MAFB, MEF2A, MEF2C, MEIS1, MITF, MNT, MYB, PRDM1, PU.1, RUNX1, SMAD3, SP1, SP2, STAT3, STAT4, TCF12, USF1, USF2, ZEB2, ZNF341, ZNF711	BCL11A, CLOCK, EGR1, FRA1, MEF2C, MEIS1, ZEB2

DAR: differential accessibility regions; DHMR: differential histone modification regions

For the *Vibrio in vitro* stimulation, interconnected clusters of TFs associated with hemopoiesis and immune functions, particularly myeloid leukocyte differentiation, FGF signalling pathway, regulation of neutrophil differentiation, lymphocyte activation, apoptosis and the ERK1/2 immune signalling, were identified. For the *Vibrio in vivo* stimulation, we detected clusters of TFs associated with similar functions (e.g. hemopoiesis, the ERK1/2 signalling pathway, myeloid cell development and cell death), but also other functions such as insulin signalling, regeneration, and oestrogen-dependent expression (Figure 7). Finally for the poly I:C *in vivo* stimulation, myeloid leukocyte differentiation, regulation of cell differentiation, cell morphogenesis and biosynthesis and growth showed connected TF subsets.

Using the Integrative Genomics Viewer (IGV), we visualized the variation in chromatin states around the promoters of 12 TF-DEGs selected from Table 5 to show the variance in chromatin state distribution across TFs and their regulatory elements following activation by the different stimulants (Figure 8; Supplementary Figure 3).

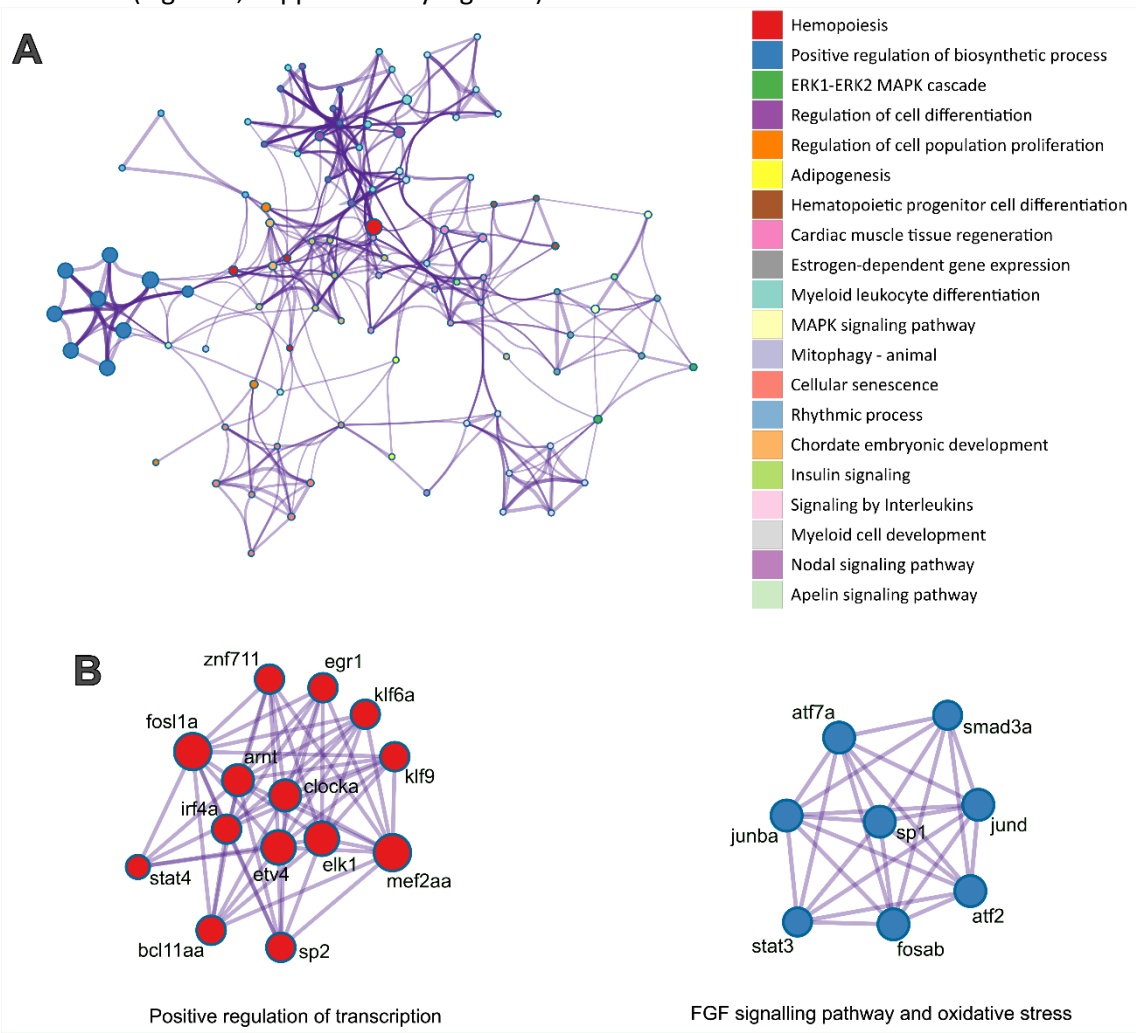

Figure 7. Functional interconnection of active TFs detected in response to the different stimulants: **A)** Ontology enrichment clusters of upregulated TFs showing promoter DARs/DHMRs with TFBMs enriched in promoter or enhancer DARs/DHMRs of DEGs detected in *Vibrio in vivo* stimulation. **B)** Protein-protein interaction MCODE network of upregulated TFs induced by *Vibrio in vivo* stimulation. Each cluster is coloured with the most statistically significant term among terms that cluster together. The size of each term is given by -log10 p, and the stronger the similarity among nearby terms, the thicker the edges between them.

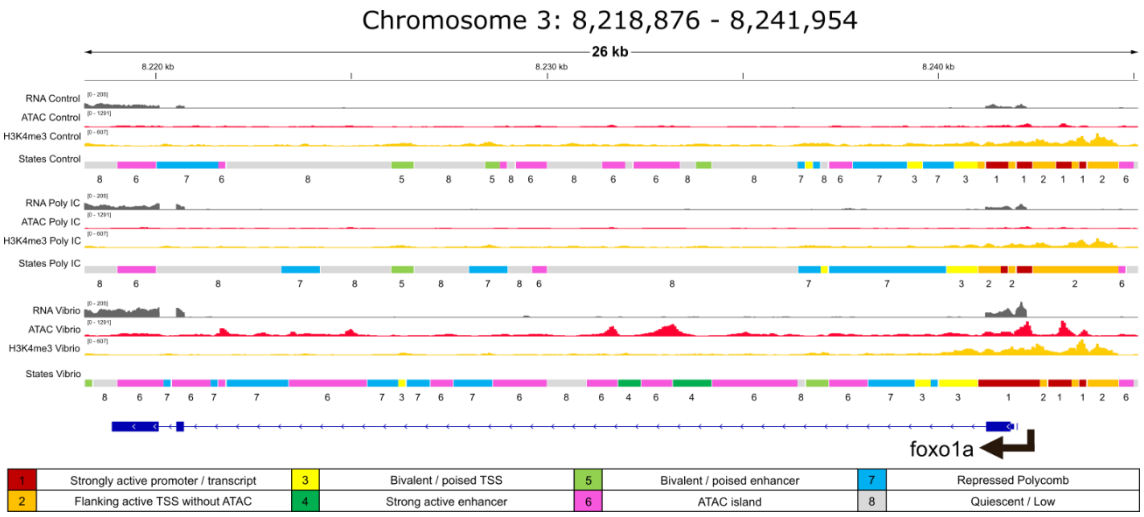

Figure 8. Chromatin state predictions and RNA/ATAC/ChIP-Seq tracks in the transcription factor coding gene *foxo1a*, which was upregulated and showed DAR around the promoter for *Vibrio in vitro* response. Transcription factor binding motifs for FOXO1A were also enriched in the promoter DARs of DEGs upregulated in response to *Vibrio in vitro*.

DISCUSSION

This study represents the first epigenomic analysis of the turbot head kidney, the primary hematopoietic and lymphoid organ of teleosts, in response to two mimics of viral (poly I:C) and bacterial (inactivated *V. anguillarum*) stimulation. While head kidney transcriptomic responses to bacteria, virus and parasites have been extensively investigated in turbot (Pardo et al., 2008; Millán et al., 2010; Domínguez et al., 2013; Díaz-Rosales et al., 2012; Robledo et al., 2014; Ronza et al., 2020; Valle et al., 2020; Libran-Pérez et al., 2022), the epigenetic regulation of chromatin states following immune stimulation has not been explored before. The head kidney response was explored through intraperitoneal injection, reflecting the response in the whole-body, including interactions among immune organs, and through *in vitro* stimulation of primary leukocyte cultures, reflecting their direct interaction with stimulants.

Transcriptomic response to immune stimulation

Upregulated genes with key immune roles were found in both *in vitro* stimulations, but also in the poly I:C *in vivo* stimulation. Poly I:C interacts with TLR3 (Toll-like receptor 3) and induces IFN production (Kumar et al., 2006). *tlr3* was upregulated in the *Vibrio in vivo* stimulation and not differentially expressed in poly I:C *in vivo*, but it was downregulated in both *in vitro* stimulations. A possible explanation is that *in vitro* downregulation could reflect signal exhaustion, suggesting that 24 hours postinjection is too long a period to capture the direct interaction between leukocytes and stimulants, and in fact, a shorter period was applied in other species with a consistent response (Herrera-Uribe et al., 2020). However, we cannot discard alternative hypotheses related to changes or diversification of the TLR3 signalling pathway in flatfish or specifically in turbot, as suggested by its activation in response to *Vibrio in vivo* stimulation and to parasites, such as *P. dicentrarchi* (Figueras et al., 2016). In fact, we identified other interferon-stimulated DEGs in poly I:C both *in vitro* and *in vivo*, including *socs1a* and b (suppressor of cytokine signalling 1), *nod2* (nucleotide binding oligomerization domain containing 2) and *nmi* (N-Myc interactor), typically participating in type I IFN responses (Blumer et al., 2017; Ahn et al., 2021). *socs1* is an inducible negative regulator of IFN (Blumer et al., 2017), a mechanism to maintain tissue homeostasis following the IFN response; *nod2* encodes for an intracellular receptor triggering innate antibacterial and antiviral signalling pathways, including IFN (Nie et

535 al., 2017); and *nmi* increases STAT-mediated transcription in response to IFN-gamma (Zhu et al.,
536 1999). The activation of genes involved in positive and negative regulation of IFN- signalling
537 suggests a fine adjustment to an intense IFN response to recover tissue homeostasis (Ivashkiv
538 and Donlin, 2014; Murira and Lamarre, 2016). Also, the upregulation of these four key genes
539 after *Vibrio in vitro* stimulation is consistent with past reports that place IFN regulation as a key
540 point of the immune response (Kopitar-Jerala, 2017).

541 Upregulated DEGs shared by both *in vivo* stimulations were involved in the activation of
542 transcription and translation and protein modification/localization. This included four members
543 of the immune-related protein arginine methyltransferase family (*prmt1*, *prmt3*, *prmt5* and
544 *prmt7*), enriched under the term "peptidyl-arginine modification". *Prmt* family members
545 regulate transcription and translation and are also involved in signal transduction during
546 inflammation and response against poly I:C and bacterial lipopolysaccharide (LPS; Srour, 2022).
547 These four genes were also shared between both *Vibrio* comparisons, suggesting an important
548 role in the early response to *Vibrio*.

549 We also checked if immune genes could be regulated in opposite directions after stimulation
550 with viral and bacterial mimics, which could reflect antagonistic immune responses. Increased
551 susceptibility to bacterial superinfections induced by innate antiviral responses has been
552 reported in several models in mammals (Barman and Metzger, 2021) in type I and type II IFN
553 responses (Navarini et al., 2006; Sun and Metzger, 2008). Such mechanisms are likely present in
554 teleosts due to the high conservation of these pathways, and in fact, different patterns of
555 resistance to viral and bacterial infections were observed among isogenic rainbow trout lines
556 (Fraslin et al., 2020). However, no negative correlations for resistance to bacteria and viruses has
557 been observed in the few studies addressing this issue in relation to selective breeding (Ødegård
558 et al., 2007; 2011; Bangera et al., 2011). Indeed, understanding the cellular basis of antagonistic
559 responses to viruses and bacteria in fish will require more research, but here we identified
560 examples of opposite gene expression responses, including genes from the core type I IFN
561 response, conserved between teleosts and humans (Levraud et al., 2019; Clark et al., 2023), such
562 as *sting1* (stimulator of interferon response CGAMP interactor 1, Zhang et al., 2021*), irf1b*
563 (interferon regulatory factor 1; Sullivan et al., 2021) and *nod2* (mentioned above),
564 downregulated by *Vibrio*s and upregulated by poly I:C *in vivo*. Reciprocally, the critical pro-
565 inflammatory cytokine *il1b* (interleukin 1 beta, Sahoo et al., 2011) and the regulator of
566 inflammation *traf4a* (TNF receptor associated factor 4, Marinis et al., 2012) were upregulated by
567 *Vibrio* but downregulated by poly I: C. Interestingly, a majority of genes induced by poly I:C and
568 repressed by *Vibrio* extracts had human/mouse ISG orthologs (22/42 *in vitro*, 18/34 *in vivo*); in
569 contrast, many genes induced by *Vibrio* extracts and repressed by poly I:C, especially *in vivo,* had
570 human/mouse orthologs downregulated by type I IFN. Overall, these observations indicate that
571 a significant part of these contrasted responses is mediated by genes functionally conserved
572 between fish and mammals.

573 **Epigenetic assays and their association with transcriptomic response**

574 Activation and recruitment of transcription factor (TF) subsets is at the top of the specific
575 transcriptome cascade response (Alvarez et al., 2020; Weidemüller et al., 2021). In our study, the
576 exploration of promoters of differentially expressed TFs, also involving differential accessibility
577 regions (DARs) and differential histone modification regions (DHMRs), barely showed changes in
578 the chromatin state distribution between treatments (Supplementary Figure 3). This is the case
579 for instance of egr*1* (early growth response 1), which plays a key role in cell survival, proliferation
580 and cell death, and regulates the expression of *il1b* and *cxcl2* (CXC motif chemokine ligand 2).

581 The same was observed for *meis1* (myeloid ecotropic viral integration site homeobox 1), related
582 to bone marrow hematopoiesis in mammals, and *zeb2* (zinc finger e-box binding homeobox 2),
583 associated with macrophage infiltration (Taylor et al., 2022). In all these examples, the TF genes
584 showed bivalent/poised promoters in the three *in vivo* samples (control, *Vibrio* and poly I:C). A
585 similar situation was found *in vitro*, where promoters of genes, such as *irf3* (interferon regulatory
586 factor 3) and *mitf* (melanocyte inducing transcription factor), showed activation signals
587 regardless of the experimental condition. In previous studies, these bivalent/poised states have
588 been interpreted as a mechanism allowing rapid responses, e.g. for genes induced during the
589 pro-inflammatory response (Herrera-Uribe et al., 2020; Martínez de Paz and Josefowicz, 2021)
590 or during mammal embryonic development and in germ cells (Lesch and Page, 2014; Barbieri et
591 al., 2017). Thus, the expression of primary response genes, such as the TF genes exemplified
592 above, may be allowed by permissive chromatin states.

593 Regardless of predicted chromatin states around gene promoters, we observed an increased
594 enrichment of these immune-related genes following poly I:C and *Vibrio* stimulation that would
595 suggest further chromatin unpacking (Table 3), even if the chromatin state is not strongly
596 affected. In fact, many differential regions were detected between stimulations, particularly
597 DARs (i.e. ATAC-Seq) and DHMRs (for H3K4me3) for *Vibrio*. In comparison, fewer DARs and
598 DHMRs were detected for the poly I:C stimulations. We interpret this absence of differential
599 regions as a return, both *in vivo* and *in vitro*, to the native chromatin state after 24 hpi, which
600 may suggest the initial response has already exhausted. Poly I:C is a synthetic double-stranded
601 RNA that acts as a PAMP binding to a specific PRR (TLR3). Meanwhile, inactive Gram-negative
602 bacteria such as *Vibrio* sp. harbour a variety of PAMPs, such as LPS, porins, peptidoglycan,
603 mannose-rich sugars and flagellin, detected by a plethora of PRRs, such as TLRs, NOD-like and C-
604 type lectin receptors, and PGRPs (Boltaña et al., 2011; Li and Wu, 2021). Thus, we explain our
605 findings as the effect of a shorter but likely intense innate response against poly I:C and a more
606 sustained response to *Vibrio*. In a previous study on pig alveolar macrophages stimulated with
607 poly I:C and LPS, Herrera-Uribe et al. (2020) noted a decrease in the number of H3K27ac-DHMRs
608 from 2 to 6 hpi, which could explain our observation in turbot (24 hpi).

609 The presence of differential activation signals at promoter regions, either in the form of open
610 chromatin regions or histone marks such as H3K4me3 and H3K27ac, are typically associated with
611 differential gene expression (Stępniak et al., 2021). H3K27ac has been widely catalogued as one
612 of the most dynamic activation marks in eukaryotes, (Saeed et al., 2014). Surprisingly, we did not
613 find important changes between experimental conditions in our study, in which H3K4me3 was
614 the most dynamic among the ChIP-Seq marks. We suspect that the decrease in H3K27ac and
615 increase in H3K4me3 could also be an effect of our choice to sample 24 hours post-injection,
616 especially for the *in vivo* stimulations. Previous studies have reported that H3K4me3 may not
617 have an active role in activating transcription, but instead reflects transcriptional changes itself,
618 suggesting that H3K4me3 modification may have role on transcriptional consistency or memory
619 of previous states (Howe et al., 2017).

620 DEG promoters overlapped with DAR/DHMRs for upregulated genes in most conditions (Table
621 4). GO enrichment of DEGs with activation signals at promoters (Supplementary table 11) was
622 similar to that observed with the whole DEG dataset (Supplementary table 5), with both *Vibrio*
623 stimulations enriched in terms associated with transcription activation, while poly I:C *in vivo*
624 showed a more specific response, enriched in immune-related processes (Supplementary table
625 6). However, DEGs of some key immune functions, such as response to cytokine stimulus, did
626 not show DAR/DHMRs, suggesting that these genes could be already accessible before

627 stimulation. Cytokines are one of the core initiators of the inflammatory response (Secombes et
628 al., 2001), thus a bivalent state, ready for activation or inactivation of expression, might explain
629 this observation (Figure 5).

630 Predicted TFBMs enriched within DARs/DHMRs in the promoters and enhancer-state regions
631 predicted by ChromHMM of upregulated DEGs, provided a more detailed picture of regulatory
632 elements changed by the immune stimulations (Figure 6, Supplementary table 12). Most of the
633 enriched TFBMs were shared between at least two treatments, which supports their general
634 regulatory function. Among those shared between most stimulations (excluding poly I:C *in vitro*),
635 we found several TFBMs of the ETS-family, which are involved in cell proliferation, apoptosis and
636 lymphocyte development (Watson et al., 2002). We also found TFBMs enrichment of PU.1, a
637 master TF for the myeloid lineage, that promotes chromatin accessibility, also identified in a
638 similar study in pig (Turkistany and DeKoter, 2011; Chen et al., 2020; Herrera-Uribe et al., 2020).
639 PU.1 is thought to promote binding of other TFs that were enriched in our study, including AP1.
640 This protein is activated by TLRs during the immune response (Shan et al., 2018) and regulates
641 gene expression in response to cytokines, stress, and bacterial and viral infections (Kim et al.,
642 2014), and notably the IFN regulatory factors (IRFs, particularly IRF3, IRF4 and IRF8). The IRFs are
643 key regulators of innate antiviral and antibacterial responses in vertebrates including fish (Clark
644 et al., 2021; Han et al., 2023). The observed ontology enrichment clustering of these TFs
645 reinforces the similarities between the conditions in our study (Figure 7, Supplementary Figure
646 2).

647 To illustrate the functionality of our turbot epigenomic atlas, we explored the chromatin state
648 changes in a selection of 12 TF genes (Figure 8, Supplementary Figure 4). These genes were
649 differentially expressed and showed DARs/DHMRs in their promoters. Immune-responsive
650 chromatin state remodelling was found, for instance, for *irf8* (interferon regulatory factor 8) in
651 the *Vibrio in vitro* stimulation. Here, an extension of the "strongly active promoter" state around
652 the TSS region was visible compared to the non-stimulated and poly I:C stimulated samples,
653 alongside an overall expansion of the "strongly active transcript" and "ATAC island" states
654 downstream. IRF8 is a key regulator of the NF-κB signalling pathway during inflammation, along
655 with IRF3 (Yan et al., 2020b). Both *irf* genes were differentially expressed in poly I:C and *Vibrio in*
656 *vitro* stimulations (*irf8* also in poly I:C *in vivo*) and showed promoter DARs in *Vibrio* stimulations.
657 Interestingly, chromatin state changes were barely observed in the vicinity of the *irf3* promoter
658 (Supplementary Figure 4).

659 Another example was found in *Vibrio* and poly I:C *in vivo* stimulations for *bcl11a* (BCL11
660 transcription factor A), a key regulator of dendritic cell differentiation (Ippolito et al., 2014) and
661 negative regulator of p53 (Yu et al., 2012). This gene was differentially expressed in both
662 stimulations, but only showed a DAR promoter in response to *Vibrio* stimulation. The
663 promoter/TSS region was annotated by ChromHMM as "weak repressed Polycomb" in the
664 control, which changed in both the *Vibrio* and poly I:C stimulations, extending to
665 "bivalent/poised" state, and in the case of *Vibrio* showing an extension to "Strongly active
666 promoter/transcript" state. Weak and strong signals of active enhancers were also detected in
667 the poly I:C and *Vibrio* stimulations within the second intron of the *bcl11a*, that were not present
668 in the controls (Supplementary Figure 4). A similar situation was found *in vitro* for *foxo1a*
669 (Forkhead box O1), a TF-coding gene that participates in mucosal (innate) immune response
670 regulating the expression of antimicrobial peptides and promoting phagocytosis during bacterial
671 and parasitic infections (Cabrera-Ortega et al., 2017; Graves and Milovanova, 2019). This gene
672 was differentially expressed in *Vibrio in vitro* and showed an extension of the "Strongly active

promoter" state compared to the control and specially the poly I:C stimulation, while conserving the "bivalent/poised TSS" stretches downstream of the promoter. This was followed by many "ATAC islands" along the gene that were also present, although more scarcely, in the control, and almost absent in poly I:C. Finally, a "medium enhancer" state was detected within the first intron, present only in the *Vibrio* condition.

Conclusions and perspectives

In summary, our study provides the first atlas of regulatory elements in turbot head kidney and leukocytes during the early response to viral and bacterial stimulation, as a contribution to the AQUA-FAANG project within the umbrella of the FAANG initiative. The integration of ATAC-Seq and ChIP-Seq data suggests that changes in chromatin state distribution were not as frequent between stimulations and controls as expected. However, the presence of DARs and DHMRs between the stimulations and the controls, which broadly overlapped with DEGs, provides clear evidence for gene regulation at the epigenetic level that underpins changes in gene expression driving immune functions. Overall, this epigenomic atlas will help to decode the molecular mechanisms underlying turbot immune responses to viral and bacterial stimuli and offers a novel resource for developing selective breeding strategies for controlling diseases, one of the main concerns of turbot industry. Future work will benefit from linking the regulatory annotations generated in this study with genetic variants defined by whole genome re-sequencing (Johnston et al., 2024), to help prioritize causal genetic variants for disease resistance traits underpinned by gene expression responses to pathogens.

DATA AVAILABILITY STATEMENT

All raw RNA-Seq, ATAC-Seq and ChIP-Seq datasets can be accessed through the ENA repository under accession numbers PRJEB47933, PRJEB47934 and PRJEB57784, respectively.

AUTHOR CONTRIBUTIONS

OA: Methodology, Software, Formal analysis, Investigation, Data Curation, Visualization, Writing – original draft, Writing – review & editing; **BGP:** Methodology, Investigation, Resources, Writing – review & editing; **PRV:** Investigation, Resources, Writing – review & editing; **ABH:** Software, Formal Analysis, Data Curation, Visualization, Writing – review & editing; **JL**: Investigation, Resources, Writing – review & editing; **PD:** Software, Formal Analysis, Writing – review & editing; **DPM:** Software, Formal Analysis, Writing – review & editing; **PB**: Resources, Writing – review & editing; **DM**: Funding Acquisition, Methodology, Supervision, Resources, Writing – review & editing; **CB**: Conceptualization, Formal Analysis, Resources, Writing – review & editing, Project Administration, Supervision; **PM**: Conceptualization, Methodology, Formal Analysis, Resources, Writing – review & editing, Project Administration, Supervision.

FUNDING

This study was funded by the AQUA-FAANG project, which received funding from the European Union's Horizon 2020 research and innovation programme under grant agreement No 817923. Additional funding was provided by Xunta de Galicia local government (Spain) (ED431C 2022/33), which also supported the research fellowships of OA and PRV (refs. ED481A-2020/119 and ED481A-2020/491430, respectively). Contributions from the Roslin Institute were further supported by the BBSRC Institutional Strategic Programme grants BBS/E/D/10002070, BBS/E/D/20002174, BBS/E/RL/230001B and BBS/E/RL/230002B.

ACKNOWLEDGMENTS

We acknowledge the technical support and informatic resources provided by the Centro de Supercomputación de Galicia (CESGA). We acknowledge Professor Carolina Tafalla (INIA-CSIC) for the support given in the revision of this article.

REFERENCES

Ahn JH, Park JY, Kim DY, Lee TS, Jung DH, Kim YJ, Lee YJ, Lee YJ, Seo IS, Song EJ, Jang AR, Yang SJ, Shin SJ, Park JH (2021). **Type I Interferons Are Involved in the Intracellular Growth Control of *Mycobacterium abscessus* by Mediating NOD2-Induced Production of Nitric Oxide in Macrophages**. Frontiers in Immunology, 12. doi: 10.3389/fimmu.2021.738070.

Alvarez JM, Schinke AL, Brooks MD, Pasquino A, Leonelli L, Varala K, Safi A, Krouk G, Krapp A, Coruzzi GM (2020). **Transient genome-wide interactions of the master transcription factor NLP7 initiate a rapid nitrogen-response cascade**. *Nature Communications*, *11*(1), 1157. doi: 10.1038/s41467-020-14979-6.

Amemiya HM, Kundaje A, Boyle AP (2019). **The ENCODE Blacklist: Identification of Problematic Regions of the Genome**. *Sci Rep* 9, 9354. doi: 10.1038/s41598-019-45839-z.

Andersson L, Archibald AL, Bottema CD, Brauning R, Burgess SC, Burt DW, Casas E, Cheng HH, Clarke L, Couldrey C, Dalrymple BP, Elsik CG, Foissac S, Giuffra E, Groenen MA, Hayes BJ, Huang LS, Khatib H, Kijas JW, … Zhou H (2015). **Coordinated international action to accelerate genome-to-phenome with FAANG, the Functional Annotation of Animal Genomes project**. *Genome Biology*, *16*(1), 57. doi: 10.1186/s13059-015-0622-4.

Andrews S (2010). **FastQC: A Quality Control Tool for High Throughput Sequence Data.** Available online at: http://www.bioinformatics.babraham.ac.uk/projects/fastqc/

APROMAR (2022). **La acuicultura en España 2022**. *Asociación Empresarial de Acuicultura de España, Cádiz* (Online, accessed October 17, 2023 at www.apromar.es)

Aramburu O, Blanco A, Bouza C, Martínez P (2023). **Integration of host-pathogen functional genomics data into the chromosome-level genome assembly of turbot (*Scophthalmus maximus*)**. *Aquaculture*, 564, 739067. doi: 10.1016/j.aquaculture.2022.739067.

Bangera R, Ødegård J, Præbel AK, Mortensen A, Nielsen HM (2011). **Genetic correlations between growth rate and resistance to vibriosis and viral nervous necrosis in Atlantic cod (*Gadus morhua* L.)**. *Aquaculture*, 317(1–4), 67–73. doi: 10.1016/j.aquaculture.2011.04.018.

Baranasic D, Hörtenhuber M, Balwierz PJ, Zehnder T, Mukarram AK, Nepal C, Várnai C, Hadzhiev Y, Jimenez-Gonzalez A, Li N, Wragg J, D'Orazio FM, Relic D, Pachkov M, Díaz N, Hernández-Rodríguez B, Chen Z, Stoiber M, Dong M, Stevens I, Ross SE, Eagle A, Martin R, Obasaju O, … Müller F (2022). **Multiomic atlas with functional stratification and developmental dynamics of zebrafish cis-regulatory elements**. *Nat Genet* 54, 1037–1050 (2022). doi: 10.1038/s41588-022-01089-w.

Barbieri M, Xie SQ, Torlai-Triglia E, Chiariello AM, Bianco S, de Santiago I, Branco MR, Rueda D, Nicodemi M, Pombo A (2017). **Active and poised promoter states drive folding of the extended HoxB locus in mouse embryonic stem cells**. *Nature Structural & Molecular Biology*, *24*(6), 515–524. doi: 10.1038/nsmb.3402

Barman TK, Metzger DW (2021). **Disease Tolerance during Viral-Bacterial Co-Infections.** *Viruses*, *13*(12), 2362. doi: 10.3390/v13122362.

757 Barnett DW, Garrison EK, Quinlan AR, Strömberg MP, Marth GT (2011). **BamTools: a C++ API**
758 **and toolkit for analyzing and managing BAM files**. *Bioinformatics*, *27*(12), 1691–1692. doi:
759 10.1093/bioinformatics/btr174.

760 Blumer T, Coto-Llerena M, Duong FHT, Heim MH (2017). **SOCS1 is an inducible negative**
761 **regulator of interferon λ (IFN-λ)–induced gene expression in vivo**. *Journal of Biological*
762 *Chemistry*, *292*(43), 17928–17938. doi: 10.1074/jbc.M117.788877.

763 Boltaña S, Roher N, Goetz FW, MacKenzie SA (2011). **PAMPs, PRRs and the genomics of gram-**
764 **negative bacterial recognition in fish**. *Developmental & Comparative Immunology*, *35*(12),
765 1195–1203. doi: 10.1016/j.dci.2011.02.010.

766 Boltsis I, Grosveld F, Giraud G, Kolovos P (2021). **Chromatin Conformation in Development and**
767 **Disease**. *Frontiers in Cell and Developmental Biology*, 9. doi: 10.3389/fcell.2021.723859.

768 Buenrostro JD, Wu B, Chang HY, Greenleaf WJ (2015). **ATAC-seq: A Method for Assaying**
769 **Chromatin Accessibility Genome-Wide**. *Current Protocols in Molecular Biology*, 109(1). doi:
770 10.1002/0471142727.mb2129s109.

771 Cabrera-Ortega AA, Feinberg D, Liang Y, Rossa C, Graves DT (2017). **The Role of Forkhead Box 1**
772 **(FOXO1) in the Immune System: Dendritic Cells, T Cells, B Cells, and Hematopoietic Stem Cells**.
773 *Critical Reviews in Immunology*, *37*(1), 1–13. doi: 10.1615/CritRevImmunol.2017019636.

774 Chen S, Yang J, Wei Y, Wei X (2020). **Epigenetic regulation of macrophages: from homeostasis**
775 **maintenance to host defense**. *Cellular & Molecular Immunology*, *17*(1), 36–49. doi:
776 10.1038/s41423-019-0315-0.

777 Chen W, Huang J, Wang W, Wang Y, Chen H, Wang Q, Zhang Y, Liu Q, Yang D (2022). **Multi-tissue**
778 **scRNA-seq reveals immune cell landscape of turbot (*Scophthalmus maximus*)**. *Fundamental*
779 *Research*, *2*(4), 550–561. doi: 10.1016/j.fmre.2021.12.015.

780 Clark EL, Archibald AL, Daetwyler HD, Groenen MAM, Harrison PW, Houston RD, Kühn C, Lien S,
781 Macqueen DJ, Reecy JM, Robledo D, Watson M, Tuggle CK, Giuffra E (2020). **From FAANG to**
782 **fork: application of highly annotated genomes to improve farmed animal production**. *Genome*
783 *Biology*, *21*(1), 285. doi: 10.1186/s13059-020-02197-8.

784 Clark TC, Boudinot P, Collet B (2021). **Evolution of the IRF Family in Salmonids**. *Genes*, *12*(2),
785 238. doi: 10.3390/genes12020238.

786 Clark TC, Naseer S, Gundappa MK, Laurent A, Perquis A, Collet B, Macqueen DJ, Martin SAM,
787 Boudinot P (2023). **Conserved and divergent arms of the antiviral response in the duplicated**
788 **genomes of salmonid fishes.** *Genomics*, *115*(4), 110663. doi: 10.1016/j.ygeno.2023.110663.

789 Corces MR, Trevino AE, Hamilton EG, Greenside PG, Sinnott-Armstrong NA, Vesuna S, Satpathy
790 AT, Rubin AJ, Montine KS, Wu B, Kathiria A, Cho SW, Mumbach MR, Carter AC, Kasowski M,
791 Orloff LA, Risca VI, Kundaje A, Khavari PA, … Chang HY (2017). **An improved ATAC-seq protocol**
792 **reduces background and enables interrogation of frozen tissues**. *Nature Methods*, *14*(10), 959–
793 962. doi: 10.1038/nmeth.4396.

794 Cuvier O, Fierz B (2017). **Dynamic chromatin technologies: from individual molecules to**
795 **epigenomic regulation in cells**. *Nature Reviews Genetics*, 18(8), 457–472. doi:
796 10.1038/nrg.2017.28.

Danecek P, Bonfield JK, Liddle J, Marshall J, Ohan V, Pollard MO, Whitwham A, Keane T, McCarthy SA, Davies RM, Li H (2021). **Twelve years of SAMtools and BCFtools**. *GigaScience*, *10*(2). doi: 10.1093/gigascience/giab008

Díaz-Rosales P, Romero A, Balseiro P, Dios S, Novoa B, Figueras A (2012). **Microarray-Based Identification of Differentially Expressed Genes in Families of Turbot (*Scophthalmus maximus*) After Infection with Viral Haemorrhagic Septicaemia Virus (VHSV)**. *Marine Biotechnology*, 14(5), 515–529. doi:10.1007/s10126-012-9465-0.

Dobin A, Davis CA, Schlesinger F, Drenkow J, Zaleski C, Jha S, Batut P, Chaisson M, Gingeras TR (2013). **STAR: ultrafast universal RNA-seq aligner**. *Bioinformatics*, *29*(1), 15–21. doi: 10.1093/bioinformatics/bts635.

Domínguez B, Pardo BG, Noia M, Millán A, Gómez-Tato A, Martínez P, Leiro J, Lamas J (2013). **Microarray analysis of the inflammatory and immune responses in head kidney turbot leucocytes treated with resveratrol**. *International Immunopharmacology*, *15*(3), 588–596. doi: 10.1016/j.intimp.2013.01.024.

Ecker S, Pancaldi V, Valencia A, Beck S, Paul DS (2018). **Epigenetic and Transcriptional Variability Shape Phenotypic Plasticity**. *BioEssays*, *40*(2), 1700148. doi: 10.1002/bies.201700148.

Ernst J, Kellis M (2012). **ChromHMM: automating chromatin-state discovery and characterization**. *Nature Methods*, *9*(3), 215–216. doi: 10.1038/nmeth.1906.

Ewels P, Peltzer A, Fillinger S, Patel H, Alneberg J, Wilm A, Ulysse-Garcia M, Di Tommaso P, Nahnsen S (2023). **The nf-core framework for community-curated bioinformatics pipelines**. *Zenodo*. doi: 10.5281/zenodo.3240506.

Fang L, Liu S, Liu M, Kang X, Lin S, Li B, Connor EE, Baldwin RL, Tenesa A, Ma L, Liu GE, Li C (2019). **Functional annotation of the cattle genome through systematic discovery and characterization of chromatin states and butyrate-induced variations**. *BMC Biology*, 17(1), 68. doi: 10.1186/s12915-019-0687-8.

Feinberg AP (2007). **Phenotypic plasticity and the epigenetics of human disease**. *Nature*, *447*(7143), 433–440. doi: 10.1038/nature05919.

Figueras A, Robledo D, Corvelo A, Hermida M, Pereiro P, Rubiolo JA, Gómez-Garrido J, Carreté L, Bello X, Gut M, Gut IG, Marcet-Houben M, Forn-Cuní G, Galán B, García JL, Abal-Fabeiro JL, Pardo BG, Taboada X, Fernández C, … Martínez P (2016). **Whole genome sequencing of turbot (*Scophthalmus maximus*; *Pleuronectiformes*): a fish adapted to demersal life**. *DNA Research*, 23(3), 181–192. doi: 10.1093/dnares/dsw007.

Foissac S, Djebali S, Munyard K, Vialaneix N, Rau A, Muret K, Esquerré D, Zytnicki M, Derrien T, Bardou P, Blanc F, Cabau C, Crisci,E, Dhorne-Pollet S, Drouet F, Faraut T, Gonzalez I, Goubil A, Lacroix-Lamandé S, … Giuffra E (2019). **Multi-species annotation of transcriptome and chromatin structure in domesticated animals**. *BMC Biology*, 17(1), 108. doi: 10.1186/s12915-019-0726-5.

Frankish A, Carbonell-Sala S, Diekhans M, Jungreis I, Loveland JE, Mudge JM, Sisu C, Wright JC, Arnan C, Barnes I, Banerjee A, Bennett R, Berry A, Bignell A, Boix C, Calvet F, Cerdán-Vélez D, Cunningham F, Davidson C, … Flicek P (2023). **GENCODE: reference annotation for the human**

and mouse genomes in 2023. *Nucleic Acids Research*, *51*(D1), D942–D949. doi: 10.1093/nar/gkac1071

Fraslin C, Quillet E, Rochat T, Dechamp N, Bernardet JF, Collet B, Lallias D, Boudinot P (2020). **Combining Multiple Approaches and Models to Dissect the Genetic Architecture of Resistance to Infections in Fish**. *Frontiers in Genetics*, 11. doi: 10.3389/fgene.2020.00677.

Gao Y, Wang Q, Liu Y, Ma Y, Jin H, Liu J, Wang H, Yan Y, Li J (2023). **Epidemiology of turbot bacterial diseases in China between October 2016 and December 2019**. *Frontiers in Marine Science*, *10*. doi: 10.3389/fmars.2023.1145083.

Ge SX, Jung D, Yao R (2020). **ShinyGO: a graphical gene-set enrichment tool for animals and plants**. *Bioinformatics*, *36*(8), 2628–2629. doi: 10.1093/bioinformatics/btz931.

Graves DT, Milovanova TN (2019). **Mucosal Immunity and the FOXO1 Transcription Factors**. *Frontiers in Immunology*, *10*. doi: 10.3389/fimmu.2019.02530.

Guerrero-Peña L, Suarez-Bregua P, Gil-Gálvez A, Naranjo S, Méndez-Martínez L, Tur R, García-Fernández P, Tena JJ, Rotllant J (2023). **Genome-wide chromatin accessibility and gene expression profiling during flatfish metamorphosis**. *Scientific Data*, *10*(1), 196. doi: 10.1038/s41597-023-02111-4.

Geven EJW, Klaren PHM (2017). **The teleost head kidney: Integrating thyroid and immune signalling**. *Developmental & Comparative Immunology*, 66, 73–83. doi: 10.1016/j.dci.2016.06.025.

Giral H, Landmesser U, Kratzer A (2018). **Into the Wild: GWAS Exploration of Non-coding RNAs**. *Frontiers in Cardiovascular Medicine*, 5. doi: 10.3389/fcvm.2018.00181.

Giuffra E, Tuggle CK (2019). **Functional Annotation of Animal Genomes (FAANG): Current Achievements and Roadmap**. *Annual Review of Animal Biosciences*, *7*(1), 65–88. doi: 10.1146/annurev-animal-020518-114913.

Halstead MM, Ma X, Zhou C, Schultz RM, Ross PJ (2020). **Chromatin remodelling in bovine embryos indicates species-specific regulation of genome activation**. *Nature Communications*, 11(1), 4654. doi: 10.1038/s41467-020-18508-3.

Halstead MM, Islas-Trejo A, Goszczynski DE, Medrano JF, Zhou H, Ross PJ (2021). **Large-Scale Multiplexing Permits Full-Length Transcriptome Annotation of 32 Bovine Tissues from a Single Nanopore Flow Cell**. *Frontiers in Genetics*, 12. doi: 10.3389/fgene.2021.664260.

Han C, Huang W, Peng S, Zhou J, Zhan H, Li W, Gong J, Li Q (2023). **Characterization and expression analysis of the interferon regulatory factor (IRF) gene family in zig-zag eel (*Mastacembelus armatus*) against *Aeromonas veronii* infection**. *Developmental & Comparative Immunology*, *140*, 104622. doi: 10.1016/j.dci.2022.104622.

He P, Williams BA, Trout D, Marinov GK, Amrhein H, Berghella L, Goh ST, Plajzer-Frick I, Afzal V, Pennacchio LA, Dickel DE, Visel A, Ren B, Hardison RC, Zhang Y, Wold BJ (2020). **The changing mouse embryo transcriptome at whole tissue and single-cell resolution**. *Nature*, *583*(7818), 760–767. doi: 10.1038/s41586-020-2536-x.

Heinz S, Benner C, Spann N, Bertolino E, Lin YC, Laslo P, Cheng JX, Murre C, Singh H, Glass CK (2010). **Simple Combinations of Lineage-Determining Transcription Factors Prime cis-**

Regulatory Elements Required for Macrophage and B Cell Identities. *Molecular Cell*, *38*(4), 576–589. doi: 10.1016/j.molcel.2010.05.004.

Herrera-Uribe J, Liu H, Byrne KA, Bond ZF, Loving CL, Tuggle CK (2020). **Changes in H3K27ac at Gene Regulatory Regions in Porcine Alveolar Macrophages Following LPS or PolyIC Exposure**. Frontiers in Genetics, 11. doi: 10.3389/fgene.2020.00817.

Howe FS, Fischl H, Murray SC, Mellor J (2017). **Is H3K4me3 instructive for transcription activation?** *BioEssays*, *39*(1), e201600095. doi: 10.1002/bies.201600095.

Hu J, Barrett RDH (2017). **Epigenetics in natural animal populations**. *Journal of Evolutionary Biology*, *30*(9), 1612–1632. doi: 10.1111/jeb.13130.

Ippolito GC, Dekker JD, Wang YH, Lee BK, Shaffer AL, Lin J, Wall JK, Lee BS, Staudt LM, Liu YJ, Iyer VR, Tucker HO (2014). **Dendritic cell fate is determined by BCL11A**. *Proceedings of the National Academy of Sciences*, *111*(11). doi: 10.1073/pnas.1319228111.

Ivashkiv LB, Donlin LT (2014). **Regulation of type I interferon responses**. *Nature Reviews Immunology*, 14(1), 36–49. doi:10.1038/nri3581.

Johnston IA, Kent MP, Boudinot P, Looseley M, Bargelloni L, Faggion S, Merino GA, Ilsley GR, Bobe J, Tsigenopoulos CS, Robertson J, Harrison PW, Martinez P, Robledo D, Macqueen DJ, Lien S (2024). **Advancing fish breeding in aquaculture through genome functional annotation**. *Aquaculture*, *583*, 740589. doi: 10.1016/j.aquaculture.2024.740589

Karimzadeh M, Ernst C, Kundaje A, Hoffman MM (2018). **Umap and Bismap: quantifying genome and methylome mappability**. *Nucleic Acids Research*. doi: 10.1093/nar/gky677.

Kellis M, Wold B, Snyder MP, Bernstein BE, Kundaje A, Marinov GK, Ward LD, Birney E, Crawford GE, Dekker J, Dunham I, Elnitski LL, Farnham PJ, Feingold EA, Gerstein M, Giddings MC, Gilbert D. M, Gingeras TR, Green ED, … Hardison RC (2014). **Defining functional DNA elements in the human genome**. *Proceedings of the National Academy of Sciences*, 111(17), 6131–6138. doi: 10.1073/pnas.1318948111.

Kim J, Lee KW, Lee HJ (2014). **Polyphenols Suppress and Modulate Inflammation**. In *Polyphenols in Human Health and Disease* (pp. 393–408). Elsevier. doi 10.1016/B978-0-12-398456-2.00029-3.

Klosterhoff MC, Pereira-Junio J, Rodrigues RV, Gusmão EP, Sampaio LA, Tesser MB, Romano L A (2015). **Ontogenic development of kidney, thymus and spleen and phenotypic expression of CD3 and CD4 receptors on the lymphocytes of cobia (*Rachycentroncanadum*)**. *Anais Da Academia Brasileira de Ciências*, 87(4), 2111–2121. doi: 10.1590/0001-3765201520140623.

Kopitar-Jerala N (2017). **The Role of Interferons in Inflammation and Inflammasome Activation**. *Frontiers in Immunology*, *8*. doi: 10.3389/fimmu.2017.00873.

Kumar A, Zhang J, Yu FSX (2006). **Toll-like receptor 3 agonist poly(I:C)-induced antiviral response in human corneal epithelial cells**. *Immunology*, *117*(1), 11–21. doi: 10.1111/j.1365-2567.2005.02258.x.

Lawson ND, Li R, Shin M, Grosse A, Yukselen O, Stone OA, Kucukural A, Zhu L (2020). **An improved zebrafish transcriptome annotation for sensitive and comprehensive detection of cell type-specific genes**. *ELife*, 9. doi: 10.7554/eLife.55792.

Levraud JP, Jouneau L, Briolat V, Laghi V, Boudinot P (2019). **IFN-Stimulated Genes in Zebrafish and Humans Define an Ancient Arsenal of Antiviral Immunity**. *The Journal of Immunology*, 203(12), 3361–3373. doi: 10.4049/jimmunol.1900804.

Lesch BJ, Page DC (2014). **Poised chromatin in the mammalian germ line**. *Development*, *141*(19), 3619–3626. doi: 10.1242/dev.113027.

Li H, Durbin R (2009). **Fast and accurate short read alignment with Burrows–Wheeler transform**. *Bioinformatics*, *25*(14), 1754–1760. doi: 10.1093/bioinformatics/btp324.

Li B, Dewey CN (2011). **RSEM: accurate transcript quantification from RNA-Seq data with or without a reference genome**. *BMC Bioinformatics*, *12*(1), 323. doi: 10.1186/1471-2105-12-323.

Li D, Wu M (2021). **Pattern recognition receptors in health and diseases**. *Signal Transduction and Targeted Therapy*, *6*(1), 291. doi: 10.1038/s41392-021-00687-0.

Librán-Pérez M, Pereiro P, Figueras A, Novoa B (2022). **Transcriptome Analysis of Turbot (*Scophthalmus maximus*) Infected With *Aeromonas salmonicida* Reveals a Direct Effect on Leptin Synthesis as a Neuroendocrine Mediator of Inflammation and Metabolism Regulation**. *Frontiers in Marine Science*, *9*. doi: 10.3389/fmars.2022.888115.

Liu S, Yu Y, Zhang S, Cole JB, Tenesa A, Wang T, McDaneld TG, Ma L, Liu GE, Fang L (2020). **Epigenomics and genotype-phenotype association analyses reveal conserved genetic architecture of complex traits in cattle and human**. *BMC Biology*, 18(1), 80. doi: 10.1186/s12915-020-00792-6.

Love MI, Huber W, Anders S (2014). **Moderated estimation of fold change and dispersion for RNA-seq data with DESeq2**. *Genome Biology*, *15*(12), 550. doi: 10.1186/s13059-014-0550-8.

Marinis JM, Hutti JE, Homer CR, Cobb BA, Cantley LC, McDonald C, Abbott DW (2012). **IκB Kinase α Phosphorylation of TRAF4 Downregulates Innate Immune Signaling**. *Molecular and Cellular Biology*, *32*(13), 2479–2489. doi: 10.1128/MCB.00106-12.

Maroso F, Hermida M, Millán A, Blanco A, Saura M, Fernández A, Dalla-Rovere G, Bargelloni L, Cabaleiro S, Villanueva B, Bouza C, Martínez P (2018). **Highly dense linkage maps from 31 full-sibling families of turbot (*Scophthalmus maximus*) provide insights into recombination patterns and chromosome rearrangements throughout a newly refined genome assembly**. *DNA Research*, 25(4), 439–450. doi: 10.1093/dnares/dsy015.

Martin M (2011). **Cutadapt removes adapter sequences from high-throughput sequencing reads**. *EMBnet.Journal*, *17*(1), 10. doi: 10.14806/ej.17.1.200

Martínez P (2016). **Genomics advances for boosting aquaculture breeding programs in Spain**. *Aquaculture*, *464*, 117–120. doi: 10.1016/j.aquaculture.2016.06.021.

Martínez P, Robledo D, Taboada X, Blanco A, Moser M, Maroso F, Hermida M, Gómez-Tato A, Álvarez-Blázquez B, Cabaleiro S, Piferrer F, Bouza C, Lien S, Viñas AM (2021). **A genome-wide association study, supported by a new chromosome-level genome assembly, suggests sox2 as**

954 **a main driver of the undifferentiatiated ZZ/ZW sex determination of turbot (*Scophthalmus***
955 ***maximus*)**. *Genomics*, 113(4), 1705–1718. doi: 10.1016/j.ygeno.2021.04.007.

956 Martínez de Paz A, Josefowicz S Z (2021). **Signaling-to-chromatin pathways in the immune**
957 **system**. *Immunological Reviews*, *300*(1), 37–53. doi: 10.1111/imr.12955.

958 Millán A, Gómez-Tato A, Fernández C, Pardo BG, Álvarez-Dios JA, Calaza M, Bouza C, Vázquez M,
959 Cabaleiro S, Martínez P (2010). **Design and Performance of a Turbot (*Scophthalmus maximus*)**
960 **Oligo-microarray Based on ESTs from Immune Tissues**. *Marine Biotechnology*, *12*(4), 452–465.
961 doi: 10.1007/s10126-009-9231-0.

962 Millán A, Gómez-Tato A, Pardo BG, Fernández C, Bouza C, Vera M, Alvarez-Dios JA, Cabaleiro S,
963 Lamas J, Lemos ML, & Martínez P (2011). **Gene Expression Profiles of the Spleen, Liver, and**
964 **Head Kidney in Turbot (*Scophthalmus maximus*) Along the Infection Process with *Aeromonas***
965 ***salmonicida* Using an Immune-Enriched Oligo-microarray**. *Marine Biotechnology*, 13(6), 1099–
966 1114. doi: 10.1007/s10126-011-9374-7.

967 Mishra S, Das R, Swain P (2018). **Status of Fish Diseases in Aquaculture and Assessment of**
968 **Economic Loss Due to Disease**; Today and Tomorrow's Printers and Publishers: New Delhi, India,
969 Volume 1.

970 Moazed D (2011). **Mechanisms for the Inheritance of Chromatin States**. *Cell*, 146(4), 510–518.
971 doi: 10.1016/j.cell.2011.07.013.

972 Mokhtar DM, Zaccone G, Alesci A, Kuciel M, Hussein MT, Sayed RKA (2023). **Main Components**
973 **of Fish Immunity: An Overview of the Fish Immune System**. *Fishes*, *8*(2), 93. doi:
974 10.3390/fishes8020093.

975 Murira A, Lamarre A (2016). **Type-I Interferon Responses: From Friend to Foe in the Battle**
976 **against Chronic Viral Infection**. *Frontiers in Immunology*, 7. doi: 10.3389/fimmu.2016.00609.

977 Navarini AA, Recher M, Lang KS, Georgiev P, Meury S, Bergthaler A, Flatz L, Bille J, Landmann R,
978 Odermatt B, Hengartner H, Zinkernagel RM (2006). **Increased susceptibility to bacterial**
979 **superinfection as a consequence of innate antiviral responses**. *Proceedings of the National*
980 *Academy of Sciences*, 103(42), 15535–15539. doi: 10.1073/pnas.0607325103.

981 Nie L, Xu XX, Xiang LX, Shao JZ, Chen J (2017). **Mutual Regulation of NOD2 and RIG-I in Zebrafish**
982 **Provides Insights into the Coordination between Innate Antibacterial and Antiviral Signaling**
983 **Pathways**. *International Journal of Molecular Sciences*, *18*(6), 1147. doi: 10.3390/ijms18061147.

984 Ødegård J, Olesen I, Gjerde B, Klemetsdal G (2007). **Positive genetic correlation between**
985 **resistance to bacterial (furunculosis) and viral (infectious salmon anaemia) diseases in farmed**
986 **Atlantic salmon (*Salmo salar*)**. *Aquaculture,* *2*71(1–4), 173–177. doi:
987 10.1016/j.aquaculture.2007.06.006.

988 Ødegård J, Baranski M, Gjerde B, Gjedrem T (2011**). Methodology for genetic evaluation of**
989 **disease resistance in aquaculture species: challenges and future prospects.** *Aquaculture*
990 *Research*, 42, 103–114. doi: 10.1111/j.1365-2109.2010.02669.x.

Overbey EG, Ng TT, Catini P, Griggs LM, StewartP, Tkalcic S, Hawkins RD, Drechsler Y (2021). **Transcriptomes of an Array of Chbiicken Ovary, Intestinal, and Immune Cells and Tissues**. *Frontiers in Genetics*, 12. doi: 10.3389/fgene.2021.664424.

Pan Z, Yao Y, Yin H, Cai Z, Wang Y, Bai L, Kern C, Halstead M, Chanthavixay G, Trakooljul N, Wimmers K, Sahana G, Su G, Lund MS, Fredholm M, Karlskov-Mortensen P, Ernst CW, Ross P, Tuggle CK, … Zhou H (2021). **Pig genome functional annotation enhances the biological interpretation of complex traits and human disease**. *Nature Communications*, 12(1), 5848. doi: 10.1038/s41467-021-26153-7.

Pan Z, Wang Y, Wang M, Wang Y, Zhu X, Gu S, Zhong C, An L, Shan M, Damas J, Halstead MM, Guan D, Trakooljul N, Wimmers K, Bi Y, Wu S, Delany ME, Bai X, Cheng HH, … Zhou H (2023). **An atlas of regulatory elements in chicken: A resource for chicken genetics and genomics**. *Science Advances*, 9(18). doi: 10.1126/sciadv.ade1204.

Pardo BG, Fernández C, Millán A, Bouza C, Vázquez-López A, Vera M, Alvarez-Dios JA, Calaza M, Gómez-Tato A, Vázquez M, Cabaleiro S, Magariños B, Lemos ML, Leiro JM, Martínez P (2008). **Expressed sequence tags (ESTs) from immune tissues of turbot (*Scophthalmus maximus*) challenged with pathogens**. *BMC Veterinary Research*, *4*(1), 37. doi: 10.1186/1746-6148-4-37.

Pardo BG, Millán A, Gómez-Tato A, Fernández C, Bouza C, Alvarez-Dios JA, Cabaleiro S, Lamas J, Leiro JM, Martínez P (2012). **Gene Expression Profiles of Spleen, Liver, and Head Kidney in Turbot (*Scophthalmus maximus*) Along the Infection Process with *Philasterides dicentrarchi* Using an Immune-Enriched Oligo-Microarray**. *Marine Biotechnology*, 14(5), 570–582. doi: 10.1007/s10126-012-9440-9.

Park PJ (2009). **ChIP–seq: advantages and challenges of a maturing technology**. *Nature Reviews Genetics*, 10(10), 669–680. doi: 10.1038/nrg2641.

Patel H, Ewels P, Peltzer A, Botvinnik O, Sturm G, Moreno D, Vemuri P, Garcia MU, Morins S, Pantano L, Binzer-Panchal M, Syme R, Zepper M, Kelly G, Hanssen F, Fellows Yates JA, Cheshire C, Espinosa-Carrasco J, Miller E, Talbot A, Zhou P, Guinchard S, Hörtenhuber M, Gabernet G, Mertes C, Straub D, Di Tommaso P (2023). **nf-core/rnaseq: nf-core/rnaseq v3.10.1 – Plastered Rhodium Rudolph**. *Zenodo*. doi: 10.5281/zenodo.7505987.

Prowse-Wilkins CP, Wang J, Xiang R, Garner JB, Goddard ME, Chamberlain AJ (2021). **Putative Causal Variants Are Enriched in Annotated Functional Regions From Six Bovine Tissues**. *Frontiers in Genetics*, *12*. doi: 10.3389/fgene.2021.664379.

Raghavan V, Kraft L, Mesny F, Rigerte L (2022). **A simple guide to *de novo* transcriptome assembly and annotation**. *Briefings in Bioinformatics*, 23(2). doi: 10.1093/bib/bbab563.

Ramberg S, Høyheim B, Østbye TKK, Andreassen R (2021). **A *de novo* Full-Length mRNA Transcriptome Generated from Hybrid-Corrected PacBio Long-Reads Improves the Transcript Annotation and Identifies Thousands of Novel Splice Variants in Atlantic Salmon**. *Frontiers in Genetics*, 12. doi: 10.3389/fgene.2021.656334.

Ramírez F, Dündar F, Diehl S, Grüning BA, Manke T (2014). **deepTools: a flexible platform for exploring deep-sequencing data**. *Nucleic Acids Research*, *42*(W1), W187–W191. doi: 10.1093/nar/gku365.

Robinson JT, Thorvaldsdottir H, Turner D, Mesirov JP (2023). **igv.js: an embeddable JavaScript implementation of the Integrative Genomics Viewer (IGV)**. *Bioinformatics*, *39*(1). doi: 10.1093/bioinformatics/btac830.

Robledo D, Ronza P, Harrison PW, Losada AP, Bermúdez R, Pardo BG, José-Redondo M, Sitjà-Bobadilla A, Quiroga MI, Martínez P (2014). **RNA-seq analysis reveals significant transcriptome changes in turbot (*Scophthalmus maximus*) suffering severe enteromyxosis**. *BMC Genomics*, 15(1), 1149. doi: 10.1186/1471-2164-15-1149.

Robledo D, Martin AP, Álvarez-Dios JA, Bouza C, Pardo BG, Martínez P (2017). **First characterization and validation of turbot microRNAs**. *Aquaculture*, 472, 76–83. do: 10.1016/j.aquaculture.2016.05.002.

Ronza P, Robledo D, Bermúdez R, Losada AP, Pardo BG, Sitjà-Bobadilla A, Quiroga MI, Martínez P (2016). **RNA-seq analysis of early enteromyxosis in turbot (*Scophthalmus maximus*): new insights into parasite invasion and immune evasion strategies**. *International Journal for Parasitology*, 46(8), 507–517. doi: 10.1016/j.ijpara.2016.03.007.

Ronza P, Robledo D, Losada AP, Bermúdez R, Pardo BG, Martínez P, Quiroga MI (2020). **The Teleost Thymus in Health and Disease: New Insights from Transcriptomic and Histopathological Analyses of Turbot, *Scophthalmus maximus***. *Biology*, *9*(8), 221. doi: 10.3390/biology9080221.

Saeed S, Quintin J, Kerstens HHD, Rao NA, Aghajanirefah A, Matarese F, Cheng SC, Ratter J, Berentsen K, van der Ent MA, Sharifi N, Janssen-Megens EM, ter Huurne M, Mandoli A, van

Sahoo M, Ceballos-Olvera I, del Barrio L, Re F (2011). **Role of the Inflammasome, IL-1β, and IL-18 in Bacterial Infections**. *The Scientific World JOURNAL*, *11*, 2037–2050. doi: 10.1100/2011/212680.

Saura M, Carabaño MJ, Fernández A, Cabaleiro S, Doeschl-Wilson AB, Anacleto O, Maroso F, Millán A, Hermida M, Fernández C, Martínez P, Villanueva B (2019). **Disentangling Genetic Variation for Resistance and Endurance to Scuticociliatosis in Turbot Using Pedigree and Genomic Information**. *Frontiers in Genetics*, *10*. doi: 10.3389/fgene.2019.00539.

Secombes CJ, Wang T, Hong S, Peddie S, Crampe M, Laing KJ, Cunningham C, Zou J (2001). **Cytokines and innate immunity of fish**. *Developmental & Comparative Immunology*, *25*(8–9), 713–723. doi: 10.1016/S0145-305X(01)00032-5.

Shan S, Liu R, Jiang L, Zhu Y, Li H, Xing W, Yang G (2018). **Carp Toll-like receptor 8 (Tlr8): An intracellular Tlr that recruits TIRAP as adaptor and activates AP-1 pathway in immune response**. *Fish & Shellfish Immunology*, *82*, 41–49. doi: 10.1016/j.fsi.2018.08.001.

Stark R, Brown G (2011). **DiffBind: differential binding analysis of ChIP-Seq peak data**. *Bioconductor*. doi: 10.18129/B9.bioc.DiffBind.

Stępniak K, Machnicka MA, Mieczkowski J, Macioszek A, Wojtaś B, Gielniewski B, Poleszak K, Perycz M, Król SK, Guzik R, Dąbrowski MJ, Dramiński M, Jardanowska M, Grabowicz I, Dziedzic A, Kranas H, Sienkiewicz K, Diamanti K, Kotulska K, … Wilczyński B (2021). **Mapping chromatin accessibility and active regulatory elements reveals pathological mechanisms in human gliomas**. *Nature Communications*, *12*(1), 3621. doi: 10.1038/s41467-021-23922-2.

Srour N, Khan S, Richard S (2022**). The Influence of Arginine Methylation in Immunity and Inflammation**. *Journal of Inflammation Research*, *Volume 15*, 2939–2958. doi: 10.2147/JIR.S364190.

Subasinghe R, Soto D, Jia J (2009). **Global aquaculture and its role in sustainable development**. *Reviews in Aquaculture*, *1*(1), 2–9. doi: 10.1111/j.1753-5131.2008.01002.x.

Sullivan C, Soos BL, Millard PJ, Kim CH, King BL (2021). **Modeling Virus-Induced Inflammation in Zebrafish: A Balance Between Infection Control and Excessive Inflammation**. *Frontiers in Immunology*, *12*. doi: 10.3389/fimmu.2021.636623.

Summers KM, Bush SJ, Wu C, Su AI, Muriuki C, Clark EL, Finlayson HA, Eory L, Waddell LA, Talbot R, Archibald AL, Hume DA (2020). **Functional Annotation of the Transcriptome of the Pig, *Sus scrofa*, Based Upon Network Analysis of an RNAseq Transcriptional Atlas**. *Frontiers in Genetics*, 10. doi: 10.3389/fgene.2019.01355.

Sun K, Metzger DW (2008). **Inhibition of pulmonary antibacterial defense by interferon-γ during recovery from influenza infection**. *Nature Medicine*, 14(5), 558–564. doi: 10.1038/nm1765.

Taylor RS, Ruiz Daniels R, Dobie R, Naseer S, Clark TC, Henderson NC, Boudinot P, Martin SAM, Macqueen DJ (2022). **Single cell transcriptomics of Atlantic salmon (*Salmo salar* L.) liver reveals cellular heterogeneity and immunological responses to challenge by** Aeromonas salmonicida. *Frontiers in Immunology*, *13*. doi: 10.3389/fimmu.2022.984799.

Troell M, Costa-Pierce B, Stead S, Cottrell RS, Brugere C, Farmery AK, Little DC, Strand Å, Pullin R, Soto D, Beveridge M, Salie K, Dresdner J, Moraes-Valenti P, Blanchard J, James P, Yossa R, Allison E, Devaney C, Barg U (2023). **Perspectives on aquaculture's contribution to the Sustainable Development Goals for improved human and planetary health**. *Journal of the World Aquaculture Society*, 54(2), 251–342. doi: 10.1111/jwas.12946.

Tuggle CK, Giuffra E, White SN, Clarke L, Zhou H, Ross PJ, Acloque H, Reecy JM, Archibald A, Bellone RR, Boichard M, Chamberlain A, Cheng H, Crooijmans RPMA, Delany ME, Finno CJ, Groenen MAM, Hayes B, Lunney JK, … Watson M (2016). **GO-FAANG meeting: a Gathering On Functional Annotation of Animal Genomes**. *Animal Genetics*, *47*(5), 528–533. doi: 10.1111/age.12466.

Turkistany SA, DeKoter RP (2011). **The Transcription Factor PU.1 is a Critical Regulator of Cellular Communication in the Immune System**. *Archivum Immunologiae et Therapiae Experimentalis*, *59*(6), 431–440. doi: 10.1007/s00005-011-0147-9.

Valle A, Leiro JM, Pereiro P, Figueras A, Novoa B, Dirks RPH, Lamas J (2020). **Interactions between the Parasite Philasterides dicentrarchi and the Immune System of the Turbot *Scophthalmus maximus*. A Transcriptomic Analysis**. *Biology*, 9(10), 337. doi: 10.3390/biology9100337

van Berkum NL, Lieberman-Aiden E, Williams L, Imakaev M, Gnirke A, Mirny LA, Dekker J, Lander ES (2010). **Hi-C: A Method to Study the Three-dimensional Architecture of Genomes**. *Journal of Visualized Experiments*, 39. doi: 10.3791/1869.

Villar D, Frost S, Deloukas P, Tinker A (2020). **The contribution of non-coding regulatory elements to cardiovascular disease**. *Open Biology*, *10*(7). doi: 10.1098/rsob.200088.

Vu H, Ernst J (2022). **Universal annotation of the human genome through integration of over a thousand epigenomic datasets**. *Genome Biology*, *23*(1), 9. doi: 10.1186/s13059-021-02572-z.

Watson DK, Li R, Sementchenko VI, Mavrothalassitis G, Seth A (2002). **ETS Family of Transcription Factors**. In *Encyclopedia of Cancer* (pp. 189–196). Elsevier. doi: 10.1016/B0-12-227555-1/00078-2.

Weidemüller P, Kholmatov M, Petsalaki E, Zaugg JB (2021). **Transcription factors: Bridge between cell signaling and gene regulation**. *PROTEOMICS*, *21*(23–24). doi: 10.1002/pmic.202000034.

Xiang R, MacLeod IM, Daetwyler HD, de Jong G, O'Connor E, Schrooten C, Chamberlain AJ, Goddard ME (2021). **Genome-wide fine-mapping identifies pleiotropic and functional variants that predict many traits across global cattle populations**. *Nature Communications*, *12*(1), 860. doi: 10.1038/s41467-021-21001-0.

Xu X, Shao C, Xu H, Zhou Q, You F, Wang N, Li W, Li M, Chen S (2020). **Draft genomes of female and male turbot *Scophthalmus maximus***. *Scientific Data*, *7*(1), 90. doi: 10.1038/s41597-020-0426-6.

Yan F, Powell DR, Curtis DJ, Wong NC (2020a). **From reads to insight: a hitchhiker's guide to ATAC-seq data analysis**. *Genome Biology*, 21(1), 22. doi: 10.1186/s13059-020-1929-3.

Yan X, Zhao X, Huo R, Xu T (2020b). **IRF3 and IRF8 Regulate NF-κB Signaling by Targeting MyD88 in Teleost Fish**. *Frontiers in Immunology*, *11*. doi: 10.3389/fimmu.2020.00606.

Yu Y, Wang J, Khaled W, Burke S, Li P, Chen X, Yang W, Jenkins NA, Copeland NG, Zhang S, Liu P (2012). **Bcl11a is essential for lymphoid development and negatively regulates p53**. *Journal of Experimental Medicine*, *209*(13), 2467–2483. doi: 10.1084/jem.20121846.

Zhang Y, Liu T, Meyer CA, Eeckhoute J, Johnson DS, Bernstein BE, Nusbaum C, Myers RM, Brown M, Li W, Liu XS (2008). **Model-based Analysis of ChIP-Seq (MACS)**. *Genome Biology*, *9*(9), R137. doi: 10.1186/gb-2008-9-9-r137.

Zhang R, Kang R, Tang D (2021). **The STING1 network regulates autophagy and cell death**. *Signal Transduction and Targeted Therapy*, *6*(1), 208. doi: 10.1038/s41392-021-00613-4.

Zhou Y, Zhou B, Pache L, Chang M, Khodabakhshi AH, Tanaseichuk O, Benner C, Chanda SK (2019). **Metascape provides a biologist-oriented resource for the analysis of systems-level datasets**. *Nature Communications*, *10*(1), 1523. doi: 10.1038/s41467-019-09234-6.

Zhu M, John S, Berg M, Leonard WJ (1999). **Functional Association of Nmi with Stat5 and Stat1 in IL-2- and IFN γ-Mediated Signaling**. *Cell*, *96*(1), 121–130. doi: 10.1016/S0092-8674(00)80965-4.

Zhu XN, Wang YZ, Li C, Wu HY, Zhang R, Hu XX. (2023). **Chicken chromatin accessibility atlas accelerates epigenetic annotation of birds and gene fine-mapping associated with growth traits**. *Zoological Research*, 44(1), 53–62. doi: 10.24272/j.issn.2095-8137.2022.228.